7-2020

Effects of Terrestrial Weathering on Rare Earth Element Concentrations and Sulfur Isotopic Signatures of Carbonaceous and Ordinary Chondrites

Ruby Virginia Patterson
University of Arkansas, Fayetteville

Effects of Terrestrial Weathering on Rare Earth Element Concentrations and Sulfur Isotopic Signatures of Carbonaceous and Ordinary Chondrites:

A thesis submitted in partial fulfillment
of the requirements for the degree of
Master of Science in Geology

by

Ruby Virginia Patterson
The University of Texas at San Antonio
Bachelor of Science in Geology, 2018

July 2020
University of Arkansas

This thesis is approved for recommendation to the Graduate Council.

_____
Adriana Potra, Ph.D.
Thesis Advisor

_____
Vincent Chevrier, Ph.D.
Committee Member

_____
Philip Hays, Ph.D.
Committee Member

_____
Barry Shaulis, Ph.D.
Committee Member

ABSTRACT

Understanding the effects of weathering of chondrites is essential to gaining accurate and useful information about the formation of our solar system, as well as a more detailed account of the mobilization of chondritic compounds when they encounter terrestrial conditions. Elemental concentrations and stable isotope analyses of chondrites, considered to be the most primordial material in the solar system, are two tools which help unlock the weathering patterns of these specimens when they enter the earth system. However, it is not currently known exactly how time spent in the field alters rare earth element (REE) concentration or $\delta^{34}S$ signatures within carbonaceous and ordinary chondrites. This study shows that REE concentration is an ineffective way to determine residence time. There are no meaningful trends identified throughout the exhaustive display of the REE results. However, the current data suggest entry to the earth system fractionates sulfur within chondrites and produces variable $\delta^{34}S$. The main result of the sulfur study shows chondrite falls are not fractionated with respect to $\delta^{34}S$ with a tight range of results which span from -0.32‰ to 1.74‰, while chondrite finds contain a wide variety of $\delta^{34}S$ signatures ranging from -0.5‰ to 5.45‰. This finding suggests the longer amount of time spent within the earth system will fractionate the sulfur species considerably within chondritic material due to exposure to aqueous fluids, temperature fluctuations, and microbiotic interaction. A better understanding of the relationship between residence time and $\delta^{34}S$ values may enable stable isotopic analyses of sulfur to be used to support ongoing efforts to gain more insights into the behavior and fate of chondrites upon interaction with the earth system.

TABLE OF CONTENTS

I. INTRODUCTION

Chondrite meteorites are mineralogically-primitive, relatively unaltered, and undifferentiated material thought to have originated from the accretion of early solar system materials (McSween, 2003). Distinguishing features such as mineralogy, texture, and composition show these early solar system materials first formed while scattered throughout the solar nebula and were amassed into meteorite parent bodies later (White, 2013). All chondrites, irrespective of sub-class, contain the same concentrations of condensable elements as the Sun (Figure 1), within a factor of 2 (White, 2013). The type of parent source body (asteroid, comet, or planetary core) determines the type of chondrite that will be created from it. A great majority of chondrites are dislodged chunks of asteroids, but some have shown evidence of cometary origin (McSween, 2003). Some chondrites were once part of a core of an ancient planet, shown by the primitive nature of the mineral content and internal structure (Sharp, 2007).

Rare Earth Elements (REE) in Chondrites

Meteorites are sometimes referred to as "the poor man's space probe" because they contain so much information about the solar system and deliver themselves to Earth free of charge. A class of meteorites known as 'chondrites' contain grains that predate the solar system itself, as well as organic molecules that preserve the isotopic signature of space (McSween, 2003). Within their primitive ingredients, chondrites contain a wealth of elemental and isotopic information that are widely believed to offer clues to how the protosolar nebula, thought to have created our solar system, was triggered into collapse (McSween, 2003; White, 2013; Labidi, 2017).

Since the Sun comprises more than 99% of the mass of the solar system, its composition can be considered identical to that of the solar system, and to the solar nebula from which the solar system formed (White, 2013). Due to similar element concentrations and nature of their formation, chondrites are representative samples of the cloud of gas and dust from which all bodies in the solar system formed billions of years ago (Figure 1).

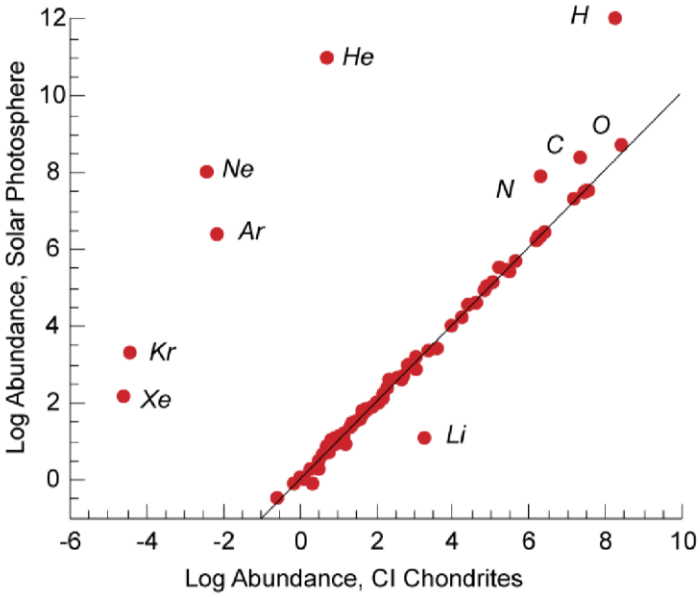

Figure 1. Abundance of elements in the Sun's photosphere vs. their abundance in the carbonaceous chondrite Orgueil (CI). Abundance of most elements agree within analytical error except non-condensing elements and Li (White, 2013).

Chondrites contain millimeter-sized silicate spherules crystallized from molten droplets known as 'chondrules' (McSween, 2003). The exact nature of chondrule formation is still largely unknown, but necessary for understanding the evolution of the early solar system. Chondrites show considerable chemical, isotopic and petrographic diversity (Grossman & Wasson, 1983; Jones, 2012) indicating that chondrule formation took place in several distinct reservoirs under widely-varying conditions. This is similar to how terrestrial rocks that are chemically, isotopically, and petrographically diverse have been created in distinct localities on Earth under different conditions. Trace element geochemistry is a powerful tool to help shed light on these

cosmogenic events. For example, Eu anomalies are consistent with magmatic fractionation encountered during planetary differentiation processes (Evensen et al, 2003). Therefore, the detection of these anomalies would offer more information to the parentage of the meteorite.

The purpose of the REE portion of this study is to identify concentration anomalies within magnetic and non-magnetic phases of carbonaceous and ordinary chondrites to constrain the nature of their formation, and highlight the mobilization of REE during terrestrial residency. The results of this study will be examined alongside results from a study of stable isotope signatures of 34-sulfur.

Sulfur in Chondrites

Sulfur (S) has four stable isotopes, making it a very useful element in geo- and cosmochemistry. Mass independent S fractionation has been observed in numerous naturally-occurring materials such as Archaean-aged sediments (Farquhar et al., 2000), inclusions in diamonds from kimberlite pipes (Farquhar et al., 2002), regolith on the Martian surface (Farquhar et al., 2000), and achondrites (Rai et al., 2005).

Sulfur components commonly exist in varying valence states (-2 to +6) within meteorites. In fact, the international standard for stable isotopic signatures of S is sourced from troilite (FeS) found in the Vienna Canyon Diablo Troilite (VCDT) iron meteorite. As the most primordial meteorite class, chondrites are the ideal candidates to posses anomalous quantities of any element. Carbonaceous chondrites contain S in four distinct forms: sulfates, sulfides, elemental sulfur, and complex organic sulfur-bearing molecules (Hoefs, 2019). However, S has been demonstrated to hold near identical values across all chondrite types (Sharp, 2007).One possible explanation for the similarity is that S was homogenously distributed throughout the solar nebula

while the Solar System was still forming. Since all chondrites are created, more or less, with identical S isotopic compositions (Figure 2), any differences observed must be due to the effects that terrestrial, biological, and geological processes impart on them.

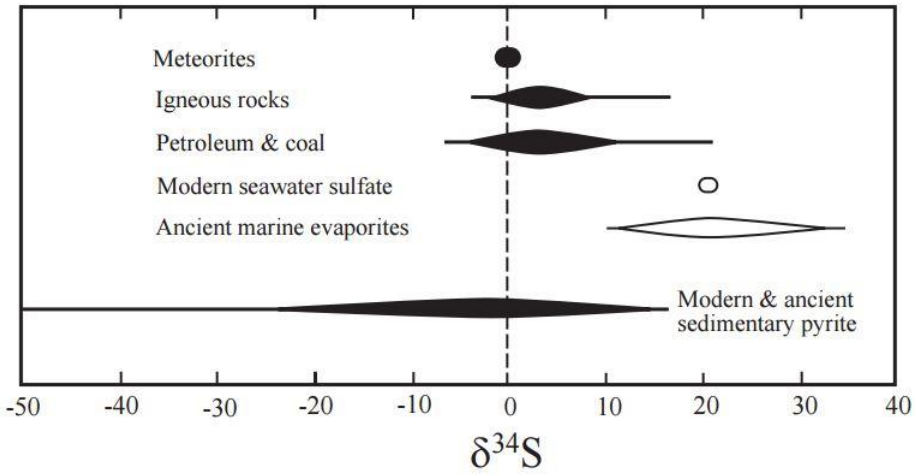

Figure 2. A comparison of possible ranges of $\delta^{34}S$ values in various geological reservoirs. Meteorites show a small range of possible $\delta^{34}S$ values compared to these reservoirs (Seal 2006).

When a meteorite falls on Earth, it is instantly subjected to geologic weathering and erosion agents just like any other terrestrially-sourced rock. After residing at the impact site for an amount of time, meteorites experience weathering and erosion that can cause extensive alteration and degradation to their physical features and chemical composition. The processes and rates of weathering in chondrites depend on the chemistry of the weathering fluid and the nature of reactions at grain surfaces (Bland, 2006). Buddhue (1957) discusses the rates of weathering being dependent upon inherent factors of the chondrite itself such as fusion crust, porosity, and composition, but also environmental factors of impact site such as moisture, temperature, carbon dioxide, soil chemistry, and vegetation. The process of meteorite weathering is essentially parent mineral phases altering to a phase that is more stable at Earth's surface. This is achieved through the breakdown of carbon-rich minerals and mobilization of sulfur-bearing compounds (Bland, 2006), which fractionate the S isotopes to form the various species of S. The

two mechanisms that alter S stable isotope ratios are kinetic effects from sulfate-reducing bacteria and temperature-dependent isotope exchange reactions that occur between sulfide mineral phases (Hoefs 2019).

The terrestrial biosphere interacts with and incorporates chemical compounds sourced from the meteoritic material for use in their life-supporting processes. Sulfate-reducing bacteria, for example, have been shown to feast on many different minerals, including sulfur-bearing phases contained within chondrites (Perkins, 2003). These bio-geo interactions preferentially incorporate lighter S isotopes from sulfur-bearing minerals in the chondrites into their biologic processes, leaving behind a heavier S isotopic signature within the remaining chondrite body (Ayangbenro et al, 1986).

Despite countless studies on chondrites, little work has been done to find a link, if any, between a chondrite's S isotopic signature and its terrestrial residence time. The stable isotopic signature of the species examined in this study, ^{34}S, is calculated using the equation:

$$\delta^{34}S = \left(\frac{\left(\frac{^{34}S}{^{32}S}\right)_{sample}}{\left(\frac{^{34}S}{^{32}S}\right)_{standard}} - 1 \right) \times 1000\ ‰$$

and will be annotated as '$\delta^{34}S$' throughout the remainder of this paper. This study will test the hypothesis that a direct relationship exists between the $\delta^{34}S$ signature of a chondrite and the length of time it has resided on Earth's surface. This will be achieved by comparing $\delta^{34}S$ values of found chondrites to those of fallen chondrites of the same classification type.

The purpose of the S isotope portion of this study is to identify $\delta^{34}S$ signature differences between fallen and found carbonaceous and ordinary chondrites to examine the effects of

weathering on found samples. The impact locations of all meteorite samples used in this study are shown in Figure 3. With a few exceptions, the samples were harvested from regions of relatively middle latitudes, implying their exposure to high temperature, humidity variations, and biota, all of which degrade the physical and chemical constitution of the samples.

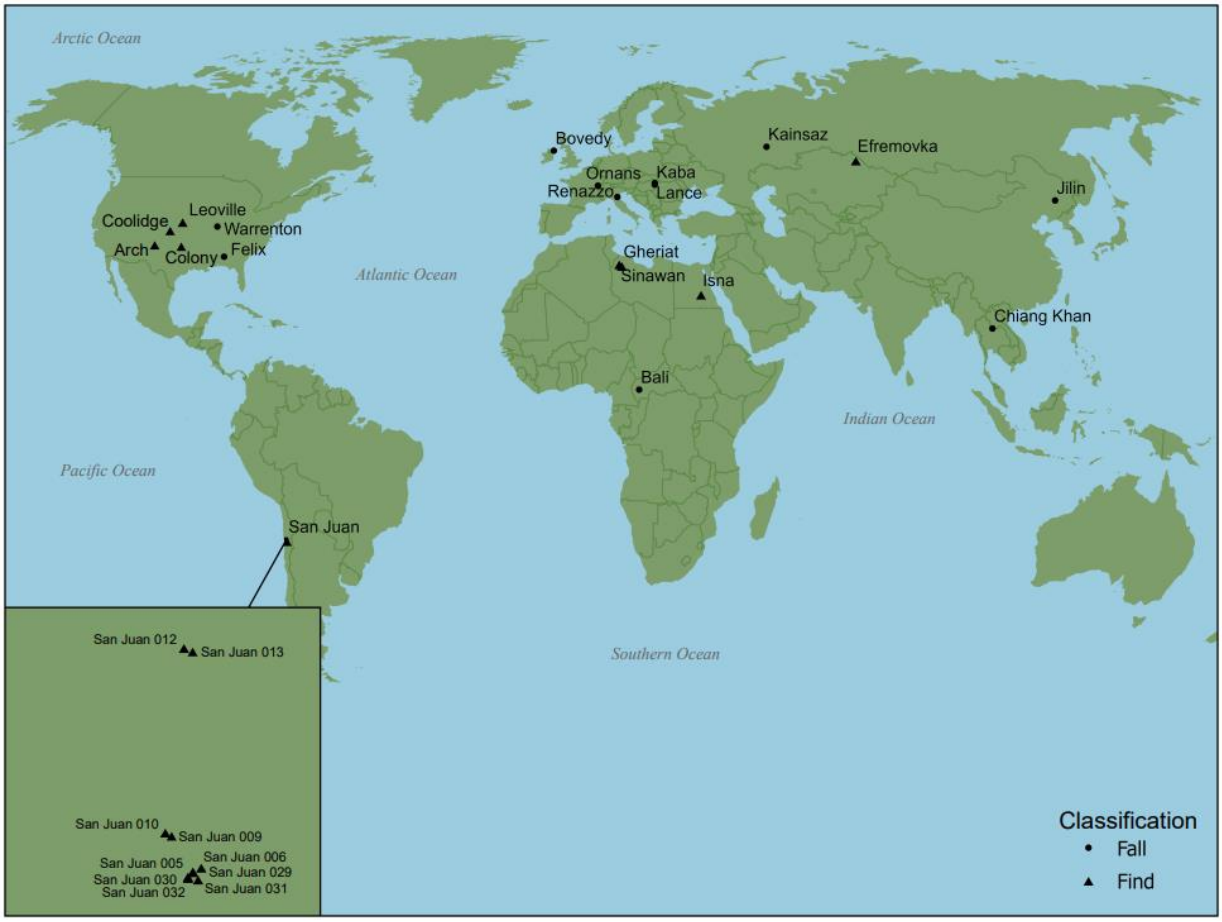

Figure 3. A global map of impact locations of the meteorites used in the S study. Falls are indicated by a circle, finds are represented by a triangle.

A prior investigation of $\delta^{34}S$ within carbonaceous chondrites was performed by Labidi et al. (2016). Sulfur was extracted from 13 carbonaceous (CM type) falls and finds. An average bulk S concentration of 2.11 ± 0.39 wt.% S (1σ) was found and no difference in bulk S abundance was detected between falls and finds. Labidi et al. (2016) only examined bulk S

abundance within CM type chondrites, whereas this study will examine the S abundance as well as isotopic signature of $\delta^{34}S$ within CO, CV, as well as O chondrites.

Rai and Thiemens (2006) conducted a study where S was extracted from different components (bulk, matrix, and chondrules) of the Dhajala (H3.8) chondrite. Leaching experiments were carried out and $\delta^{34}S$ values were determined through mass spectrometry analyses. This study found the bulk composition to contain 1.98% S by weight and $\delta^{34}S$ varying from -0.931‰ to 0.869‰ relative to Canyon Diablo Troilite (CDT). The chondrule was found to contain 0.76% S by weight and a range of $\delta^{34}S$ from -1.067‰ to 0.995‰ with respect to CDT.

Classification of Chondrites

The classification of chondrites (Table 1) depends on their chemical composition, aqueous alteration, and thermal metamorphic history. The chemical composition identifies a chondrite as ordinary, enstatite, or carbonaceous. These chemical groups are further subdivided by differing amounts of iron and the degree of oxidation. The metamorphic alteration history is classified by assigning a number 1-6 that corresponds to chondrule texture, with 1 indicating the absence of chondrules, 3-4 indicating abundant and distinct chondrules, and 6 indicating the increasingly indistinct presence of chondrules due to the effects of thermal metamorphism (Norton, 2002, and references therein). This study examines chondrites from the carbonaceous and ordinary subtypes.

Table 1. The classification scheme for chondrites (modified from White, 2013).

Chemical type			1	2	3	4	5	6
		Chondrule texture	Absent	Sparse	Abundant / distinct		Increasingly indistinct	
Ordinary chondrites	H							
	L							
	LL							
Carbonaceous chondrites	CI							
	CM							
	CR							
	CO							
	CV							
	CK							
R chondrites	R							
Enstatite chondrites	EH							
	EL					(not yet found)		

< 150°C < 200°C 400°C 600°C 700°C 750°C 950°C

Increasing aqueous alteration

Increasing thermal metamorphism

i. Carbonaceous Chondrites

The carbonaceous (C) chondrites have a carbon-rich matrix taking the form of carbonates and organic material such as amino acids (Cronin et al., 1988). They are believed to originate from rocky parent bodies mixed with ice. When the body was heated, the ice melted into liquid water, absorbed the heat, and prevented the chondrite from reaching ultra high temperatures and subsequent metamorphic alteration (Scott, 2014). Mineral phases most commonly found within carbonaceous chondrites are provided in Table 2.

a) CV Type:

Most CV chondrites belong to the petrologic type 3, indicating they have both abundant and distinct olivine chondrules (Table 1). These magnesium-rich chondrules (forsterite) are typically surrounded by iron sulfide and reside in a dark gray matrix of iron-rich olivine, fayalite (Saunier, 1998). CV meteorites also contain irregular white calcium-aluminum inclusions (CAIs)

of differing size that often make up more than 5% of the meteorite. CAIs are high-temperature minerals composed of silicates and oxides of calcium, aluminium, and titanium (Jones, 2012).

b) CO Type:

Like the CV group, most members of this group belong to the petrologic type 3. Both groups have similar chemistry and composition, leading many researchers (Jones, 2012; Scott and Krott, 2014; White, 2013) to suggest they formed in the same general region of the early solar system. One difference, however, is that CO chondrites are typically dark gray or black in color, contain smaller and fewer CAIs, and exhibit smaller chondrules (Saunier, 1998). These chondrules are packed densely within the olivine matrix and comprise roughly 70% of the entire meteorite. The opposite is true for CV chondrites, with 30% of the meteorite consisting of larger chondrules and only 70% comprised of matrix material. COs also contain tiny flakes of nickel-iron, suggesting they formed under more extreme reducing conditions than metal-devoid CVs (White, 2013).

ii. Ordinary Chondrites

The ordinary chondrites are the most abundant class of stony meteorites on Earth and are composed primarily of olivine, orthopyroxene and lesser amounts of oxidized nickel-iron alloy (Saunier, 1998; White, 2013). Additional mineral phases commonly present in ordinary chondrites are provided in Table 2. Ordinary chondrites have undergone high temperature processes, leading to melting and recrystallization. The recrystallization process erases most semblance of chondrule structure (Figure 4), limiting them to a metamorphic alteration number between 3-6 (Table 1). Ordinary chondrites are further classified by the relative abundance and

type of metals they contain: H- high iron, L- low iron, LL- low iron and overall metal (Scott, 2014).

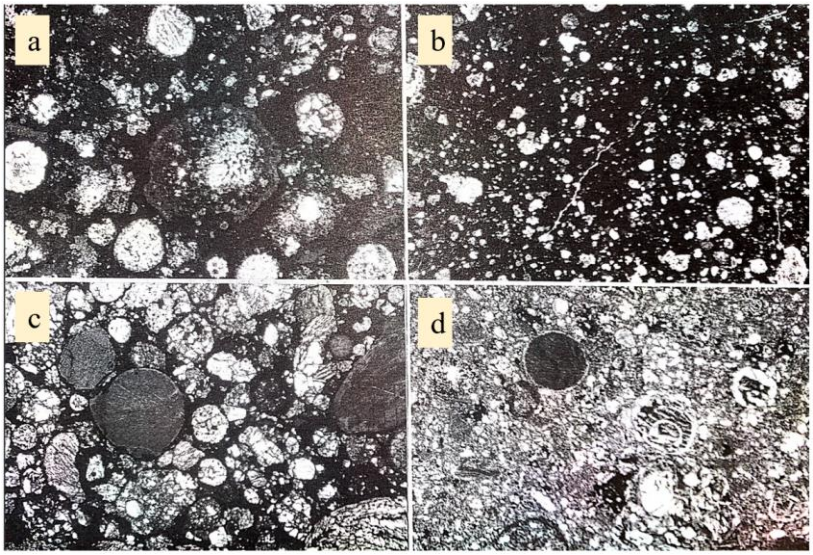

Figure 4. Optical photomicrographs of chondrites showing variations in chondrule sizes and abundances between various chondrite groups (a, b, c), and effect of metamorphism in ordinary chondrites (c, d). All photos are to the same scale, 7.25 mm across. (a) CV3 chondrite, Allende; (b) CM2 chondrite, Murchison; (c) Type 3 ordinary chondrite, Semarkona (LL3); (d) Type 5 ordinary chondrite, Tuxtuac (LL5) (modified from Brearley and Jones 1998).

Table 2. Common mineral phases found within carbonaceous and ordinary chondrites, including magnetic minerals (asterisk).

	Carbonaceous	Ordinary
Silicates	Enstatite, $MgSiO_3$ Olivine, $(Mg,Fe)_2SiO_4$ Anorthite, $CaAl_2Si_2O_8$ Nepheline, $(Na, K)AlSiO_4$ Mellilite, $(Ca,Na)_2(Al,Mg)(Si,Al)_2O_7$ Serpentine, $Mg_3Si_2O_5(OH)_4$	Enstatite, $MgSiO_3$ Olivine, $(Mg,Fe)_2SiO_4$ Anorthite, $CaAl_2Si_2O_8$ Hypersthene, $(Mg, Fe)SiO_3$ Ringwoodite, $(Mg, Fe)_2\ SiO_4$
Oxides *=magnetic	Chromite, $FeCr_2O_4$ Magnetite*, Fe_3O_4 Spinel, $MgAl_2O_4$	Chromite, $FeCr_2O_4$ Magnetite*, Fe_3O_4
Sulfides *=magnetic	Pentlandite*, $(Fe,Ni)_9S_8$ Pyrrhotite*, $Fe_{(1-x)}S$ Troilite, FeS	Pyrrhotite*, $Fe_{(1-x)}S$ Troilite, FeS
Phosphates	Whitlockite, $Ca_9MgH(PO_4)_7$	Whitlockite, $Ca_9MgH(PO_4)_7$
Carbides		Cohenite, $(Fe, Ni)_3C$
Native Elements and Metals	Awaruite, Ni_3Fe Copper, Cu	Copper, Cu Kamacite, α-(Fe, Ni)

Sample List

The definitive list of meteorites used in this study is displayed below (Table 3). The table includes details about each meteorite, such as name, type, petrologic grade, and whether the sample was found or collected shortly after a witnessed fall. The table also provides location of impact, as well as precipitation and temperature data for each impact site. An additional column, 'Both Studies?', shows whether the listed meteorite has been used in both studies (the REE concentration and the S isotope) or not. All official impact site locations were obtained through the Meteoritical Database.

Table 3. Petrologic details and impact location details of chondrites analyzed in this study.

Name	Type	Grade	Find?	Location	Lat/Long	Both Studies?	Avg Ann Precip (mm)	Avg Ann. Temp (℃)
Arch	CV	3	Y	Portales, New Mexico, USA	34°09'N / 103°13'12"W	Y	440[+]	15[+]
Bali	CV	3	N	Baoro, Central African Republic	5° 23'N / 16° 23'E	Y	1418*	24*
Bovedy	O	L3	N	Belfast, Ireland	54° 34'N / 6° 20'W	Y	976*	9*
Chiang Khan	O	H6	N	Vientiane Province, Laos	17° 54'N / 101° 38'E	Y	1622*	25.4*
Colony	CO	3	Y	Oklahoma, USA	35°21'N / 98°41'W	Y	792[+]	59[+]
Coolidge	CV	4-U	Y	Kansas, USA	38° 2'N / 101° 59'W	Y	388*	12*
Dhajala	O	H3	N	Sayla Taluka, India	22°22'40"N / 71°25'38"E	N	676[#]	31[#]
Efremovka	CV	3	Y	Pavlodar District, Kazakhstan	52° 30'N / 77° 0'E	Y	278*	2*
Farmington	O	L5	N	Kansas, USA	39° 45'N / 97° 2'W	N	836[+]	12[+]
Felix	CO	3.3	N	Alabama, USA	32° 32'N / 87° 10'W	Y	1298[+]	18[+]
Gheriat 002	O	L6	Y	Gharyan, Libya	30° 39' 30"N / 12° 18' 24"E	Y	25[$]	18[$]
Glasatovo	O	H4	N	Tverskaya oblast, Russia	57° 21'N / 37° 37'E	N	609*	4*
Isna	CO	3.8	Y	Luxor, Egypt	24° 50'N / 31° 40'E	Y	0[~]	23[~]
Jilin	O	H5	N	Jilin, China	44° 3'N / 126° 10'E	Y	679*	4*
Kaba	CV	3	N	Hajdu-Bihar, Hungary	47° 21'N / 21° 18'E	Y	566[~]	11*
Kainsaz	CO	3.2	N	Tatarstan, Russia	55° 26'N / 53° 15'E	Y	679*	5*
Karkh	O	L6	N	Balochistan, Pakistan	27° 48'N / 67° 10'E	N	225*	20.3*
Lance	CO	3.5	N	Centre, France	47° 42'N / 1° 4'E	Y	637*	11*
Leoville	CV	3	Y	Kansas, USA	39° 38' 0"N / 100° 28' 2"W	Y	1160*	15*
Limerick	O	H5	N	Munster, Ireland	52° 34'N / 8° 47'W	N	981*	10*
Malotas	O	H5	N	Malotas, Argentina	28° 56'S / 63° 14'W	N	584*	21*
Mount Browne	O	H6	N	New South Wales, Australia	29° 48'S / 141° 42'E	N	325[^]	22[^]
Ornans	CO	3.4	N	Ornans, France	47° 7'N / 6° 9'E	Y	1235*	10*
Renazzo	CR	2	N	Emilia-Romagna, Italy	44° 46'N / 11° 17'E	Y	803[~]	14*
San Juan 005 (M5)	O	H6	Y	San Juan, Chile	25°34.53'S / 69°47.7'W	Y	100*	17*
San Juan 009 (M9)	CO	3	Y	San Juan, Chile	25°30′S / 69°50′W	Y	100*	17*
San Juan 012 (M12)	O	H5	Y	San Juan, Chile	25°4.53'S / 69°47.7'W	Y	100*	17*
San Juan 029 (M29)	O	H3	Y	San Juan, Chile	25°35'S / 69°47'W	Y	100*	17*
San Juan 031 (M31)	O	L3	Y	San Juan, Chile	25°35'S / 69°47'W	Y	100*	17*
Sinawan 001	O	L6	Y	Jabal al Gharbi, Libya	31° 0'N / 11° 40'E	Y	346*	18*
Warrenton	CO	3.7	N	Missouri, USA	38° 41'N / 91° 9'W	Y	1058[+]	12[+]
References :	+: en.climate-data.org; *: usclimatedata.com; #: https://surendranagar.nic.in;							
	~: www.weather-and-climate.com; $: www.weatherspark.com; ^: www.bushmantanks.com.au							

II. RARE EARTH ELEMENT CONCENTRATION STUDY

Methodology

Chondrite (n=31) samples were crushed and separated into magnetic and non-magnetic mineral phases. Both phases of each chondrite were prepared in identical fashion. Fifteen mg of each phase were weighed using a microbalance and placed into 10 mL PFA vials that had been previously acid cleaned. Following addition of 2 mL of aqua regia (HNO_3 + 3HCl) to each sample, the vials were capped and placed on a hot plate held at 175℃ for 12 hours. After allowing to cool down completely, the vials were uncapped and the samples were allowed to dry down to completion on a hotplate at 125℃. Three more complete digestion and drying cycles were implemented with 2 mL HF, 2 mL 6.47N HCl, and 1 mL of HNO_3, respectively. Once completely digested, dried down, and cooled, the samples were diluted with 3 mL 2% HNO_3 and placed into acid cleaned 10 mL centrifuge tubes before analysis.

Table 4. The type and number of chondrites analyzed in this study for REE concentration (modified from White, 2013).

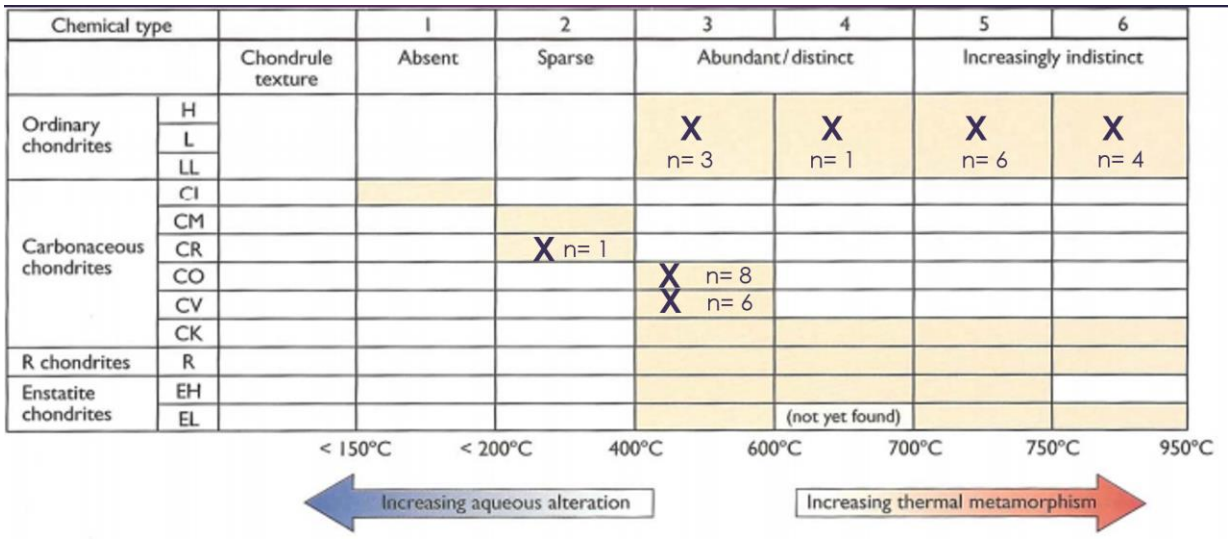

REE concentrations were determined using a Thermo Scientific iCAP Q Inductively Coupled Plasma Mass Spectrometer (ICP-MS). Raw intensity data were given for each element in both counts per second (cps) and parts per billion (ppb). Six U.S. Geological Survey rock standards (AGV-2; BHVO-2; BIR-1a; DNC-1a; QLO-1a; W-2a) were measured along with the samples to build calibration curves and constrain the accuracy and reproducibility of the measurements. The six standards were run two times in the sequence: at the beginning and at the end of the sequence. The values from the start of the sequence were used to build calibration curves. Blanks were run throughout the analyses, after each set of 12 samples, yielding very low values that account for negligible external contamination. The results showing the trace element concentrations are found in Table 5 and represented in Figure 5.

Table 5. Experimental data for the REE concentration study.

			Rare Earth Element Concentration (ppm)												
Chondrite	Type	Mag/Nonmag	Ce	Pr	Nd	Sm	Eu	Gd	Tb	Dy	Ho	Er	Tm	Yb	Lu
Arch	CV	M	0.43	0.06	0.27	0.09	0.04	0.09	0.02	0.11	0.02	0.07	0.01	0.07	0.01
		N	0.52	0.08	0.41	0.13	0.05	0.14	0.03	0.18	0.04	0.11	0.02	0.12	0.02
Bali	CV	M	0.72	0.36	1.43	0.27	0.08	0.26	0.04	0.25	0.05	0.15	0.02	0.14	0.03
		N	0.67	0.10	0.50	0.16	0.06	0.19	0.04	0.24	0.05	0.16	0.02	0.16	0.03
Bovedy	O	M	0.64	0.09	0.40	0.12	0.04	0.15	0.03	0.19	0.04	0.13	0.02	0.12	0.02
		N	0.69	0.10	0.54	0.18	0.07	0.19	0.04	0.25	0.05	0.15	0.03	0.16	0.03
Chiang Khan	O	M	9.22	1.38	7.08	2.24	0.83	2.62	0.51	3.55	0.72	2.05	0.30	1.95	0.37
		N	0.04	0.02	0.03	0.02	0.01	0.02	0.01	0.02	0.01	0.02	0.01	0.02	0.01
Colony	CO	M	0.39	0.06	0.30	0.10	0.04	0.12	0.02	0.16	0.04	0.13	0.01	0.10	0.02
		N	1.02	0.88	3.34	0.54	0.14	0.55	0.08	0.46	0.09	0.26	0.04	0.22	0.04
Coolidge	CV	M	0.91	0.14	0.70	0.23	0.09	0.27	0.05	0.35	0.07	0.22	0.03	0.21	0.04
		N	0.83	0.13	0.64	0.21	0.08	0.26	0.05	0.34	0.07	0.21	0.03	0.21	0.04
Dhajala	O	M	0.50	0.07	0.37	0.12	0.04	0.14	0.03	0.17	0.04	0.11	0.02	0.10	0.02
		N	0.57	0.09	0.44	0.14	0.05	0.17	0.03	0.23	0.05	0.15	0.02	0.14	0.03
Farmington	O	M	0.30	0.04	0.19	0.06	0.02	0.07	0.01	0.09	0.02	0.06	0.01	0.05	0.01
		N	0.76	0.11	0.55	0.18	0.05	0.21	0.04	0.27	0.06	0.17	0.03	0.16	0.03
Felix	CO	M	0.55	0.09	0.43	0.14	0.05	0.16	0.03	0.20	0.04	0.13	0.02	0.12	0.02
		N	612.69	80.07	338.25	82.71	18.53	102.15	18.48	128.40	26.82	80.66	12.63	64.74	13.20
Gheriat 002	O	M	0.55	0.07	0.36	0.11	0.03	0.12	0.02	0.15	0.03	0.10	0.01	0.09	0.02
		N	0.03	0.01	0.02	0.02	0.01	0.01	0.01	0.01	0.01	0.01	0.01	0.01	0.01
Glasatovo	O	M	0.26	0.03	0.17	0.05	0.02	0.06	0.01	0.08	0.02	0.05	0.01	0.05	0.01
		N	0.52	0.08	0.41	0.14	0.05	0.17	0.03	0.22	0.05	0.14	0.02	0.14	0.02
Isna	CO	M	0.78	0.12	0.60	0.18	0.07	0.21	0.04	0.27	0.05	0.16	0.03	0.18	0.03
		N	0.01	0.00	0.01	0.00	0.00	0.00	0.00	0.00	0.00	0.00	0.00	0.00	0.00
Jilin	O	M	0.89	0.13	0.67	0.22	0.09	0.26	0.05	0.34	0.07	0.22	0.03	0.22	0.04
		N	1.33	0.37	1.61	0.40	0.13	0.38	0.07	0.43	0.09	0.25	0.04	0.26	0.04
Kaba	CV	M	1.11	1.03	3.91	0.62	0.17	0.63	0.09	0.52	0.11	0.30	0.04	0.25	0.05
		N	0.55	0.11	0.59	0.17	0.05	0.25	0.05	0.31	0.06	0.19	0.03	0.13	0.03
Kainsaz	CO	M	0.71	0.11	0.54	0.18	0.07	0.20	0.04	0.26	0.05	0.16	0.02	0.17	0.03
		N	0.86	0.13	0.66	0.21	0.07	0.25	0.05	0.33	0.07	0.21	0.03	0.21	0.04
Karkh	O	M	0.63	0.10	0.52	0.16	0.06	0.18	0.03	0.24	0.05	0.16	0.02	0.14	0.03
		N	0.03	0.01	0.02	0.01	0.01	0.01	0.01	0.01	0.01	0.01	0.01	0.01	0.01
Lance	CO	M	0.01	0.00	0.01	0.00	0.00	0.00	0.00	0.00	0.00	0.00	0.00	0.00	0.00
		N	0.74	0.11	0.56	0.18	0.07	0.21	0.04	0.27	0.06	0.17	0.03	0.17	0.03
Leoville	CV	M	1.12	0.18	0.89	0.29	0.09	0.30	0.06	0.39	0.08	0.24	0.04	0.25	0.04
		N	2.00	0.31	1.53	0.51	0.17	0.53	0.10	0.68	0.14	0.43	0.07	0.45	0.07
Limerick	O	M	0.15	0.02	0.10	0.03	0.01	0.03	0.01	0.04	0.01	0.03	0.00	0.03	0.01
		N	1.14	0.14	0.59	0.16	0.05	0.17	0.03	0.21	0.05	0.14	0.02	0.13	0.02
Malotas	O	M	0.22	0.03	0.16	0.05	0.02	0.06	0.01	0.07	0.02	0.05	0.01	0.05	0.01
		N	0.83	0.13	0.65	0.21	0.06	0.26	0.05	0.33	0.07	0.22	0.03	0.20	0.03
Mt. Browne	O	M	0.39	0.06	0.28	0.09	0.03	0.10	0.02	0.13	0.03	0.08	0.01	0.08	0.01
		N	0.06	0.02	0.04	0.02	0.01	0.02	0.01	0.03	0.01	0.02	0.01	0.02	0.01
Ornans	CO	M	0.50	0.08	0.41	0.13	0.05	0.15	0.03	0.20	0.04	0.14	0.02	0.12	0.02
		N	0.04	0.02	0.03	0.02	0.01	0.02	0.01	0.02	0.01	0.02	0.01	0.02	0.01
Renazzo	CR	M	0.41	0.06	0.31	0.10	0.03	0.11	0.02	0.15	0.03	0.09	0.01	0.08	0.02
		N	0.02	0.00	0.07	0.00	0.00	0.00	0.00	0.00	0.00	0.00	0.00	0.00	0.00
San Juan 005	O	M	0.04	0.02	0.03	0.02	0.01	0.02	0.01	0.02	0.01	0.02	0.01	0.02	0.01
		N	0.42	0.07	0.33	0.11	0.05	0.13	0.03	0.17	0.04	0.11	0.02	0.11	0.02
San Juan 009	CO	M	0.04	0.02	0.03	0.02	0.01	0.02	0.01	0.02	0.01	0.02	0.01	0.02	0.01
		N	0.47	0.07	0.39	0.12	0.07	0.15	0.03	0.21	0.05	0.14	0.02	0.15	0.03
San Juan 012	O	M	0.05	0.02	0.03	0.02	0.01	0.02	0.01	0.02	0.01	0.02	0.01	0.02	0.01
		N	0.35	0.05	0.27	0.08	0.03	0.11	0.02	0.14	0.03	0.09	0.01	0.09	0.02
San Juan 029	O	M	0.04	0.02	0.03	0.02	0.01	0.02	0.01	0.02	0.01	0.02	0.01	0.02	0.01
		N	0.46	0.07	0.35	0.11	0.05	0.14	0.03	0.19	0.04	0.12	0.02	0.13	0.02
San Juan 031	O	M	0.50	0.08	0.38	0.12	0.05	0.15	0.03	0.20	0.04	0.13	0.02	0.12	0.02
		N	0.59	0.09	0.45	0.14	0.06	0.15	0.03	0.21	0.04	0.13	0.02	0.13	0.02
Sinawan 001	O	M	0.45	0.07	0.36	0.12	0.04	0.14	0.03	0.18	0.04	0.11	0.02	0.11	0.02
		N	0.81	0.11	0.50	0.14	0.05	0.16	0.03	0.20	0.04	0.12	0.02	0.12	0.02
Warrenton	CO	M	0.67	0.10	0.53	0.17	0.06	0.23	0.04	0.31	0.07	0.20	0.03	0.17	0.03
		N	0.70	0.11	0.56	0.18	0.07	0.21	0.04	0.27	0.06	0.18	0.03	0.16	0.03

i. Magnetic vs. Non-magnetic

a. Carbonaceous Chondrites

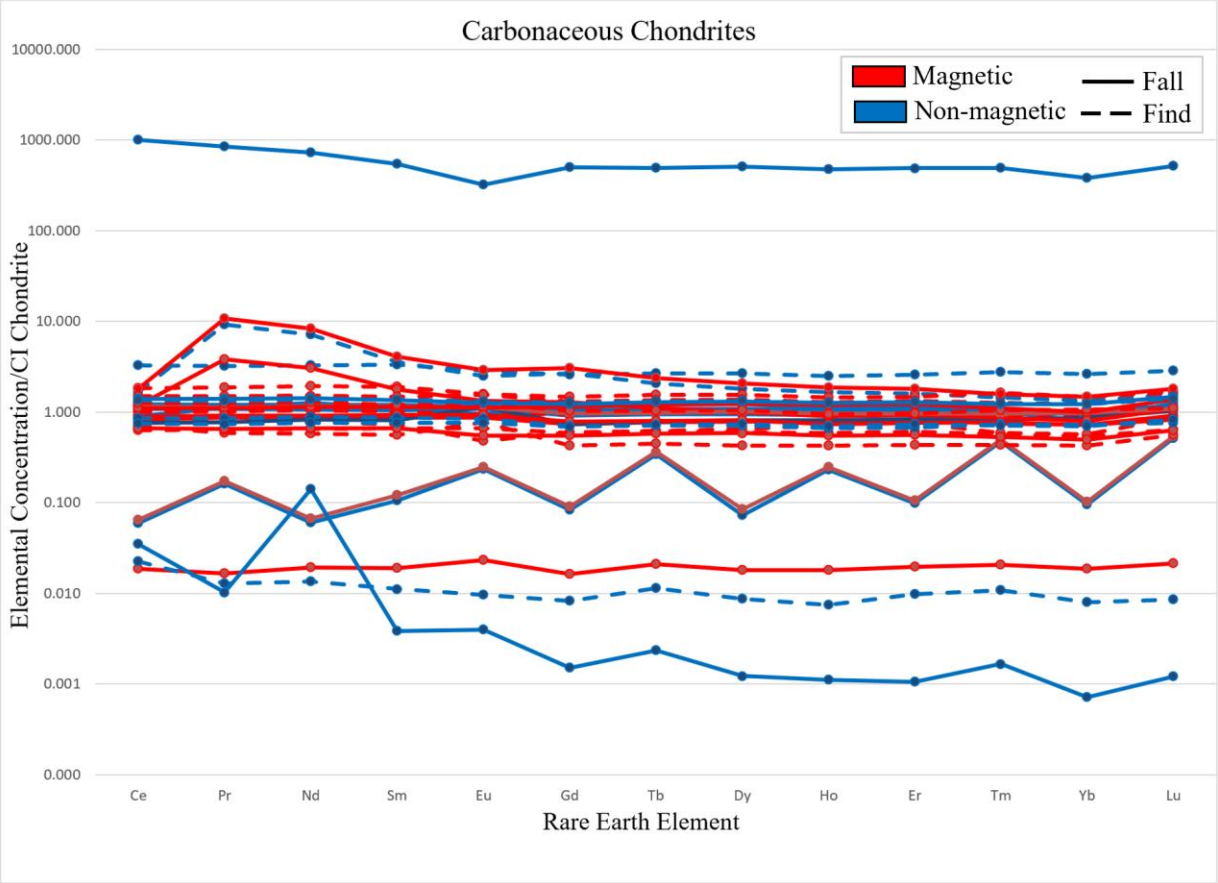

Figure 5. Chondrite normalized REE values for carbonaceous chondrites. Red and blue lines indicate the concentrations were measured on the magnetic and the non-magnetic fraction, respectively, of the samples. Solid lines are falls and dashed lines are finds.

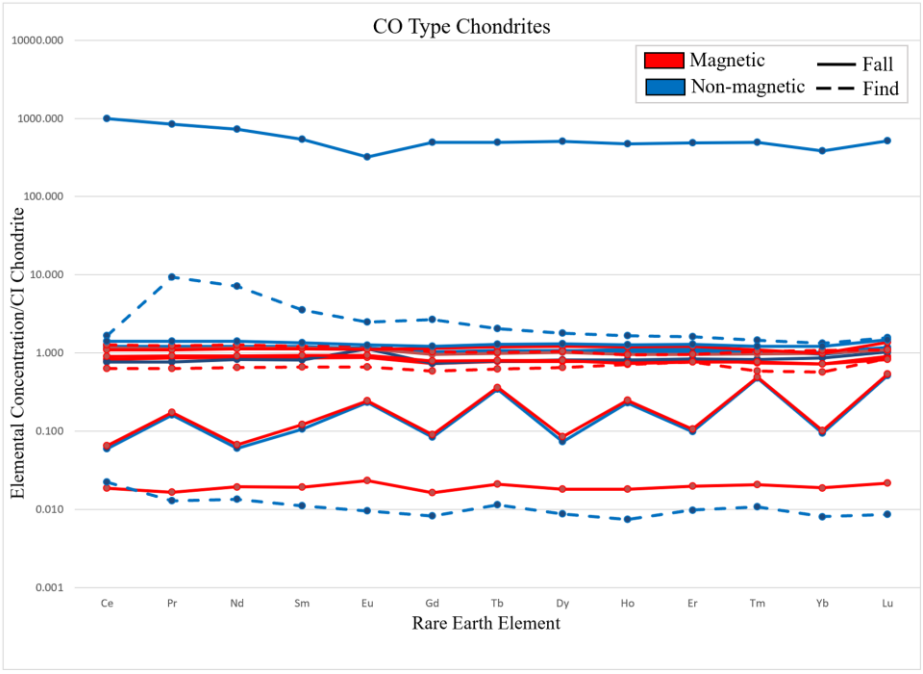

Figure 6. Chondrite normalized REE values for CO type carbonaceous chondrites. Red and blue lines indicate that the concentrations were measured on the magnetic and the non-magnetic fraction, respectively, of the samples. Solid lines are falls and dashed lines are finds.

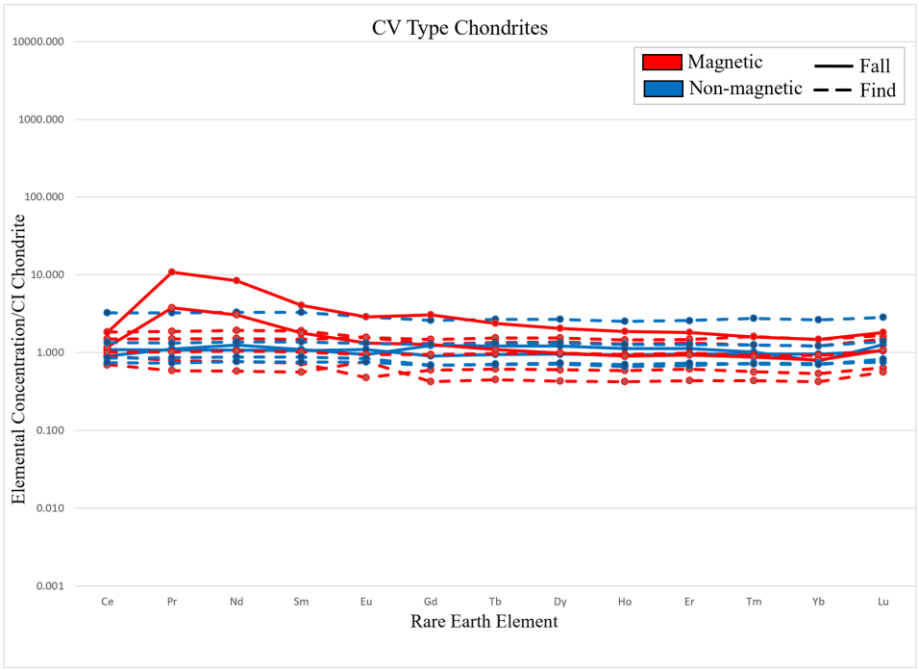

Figure 7. Chondrite normalized REE values for CV type carbonaceous chondrites. Red and blue lines indicate that the concentrations were measured on the magnetic and the non-magnetic fraction, respectively, of the samples. Solid lines are falls and dashed lines are finds.

b. Ordinary Chondrites

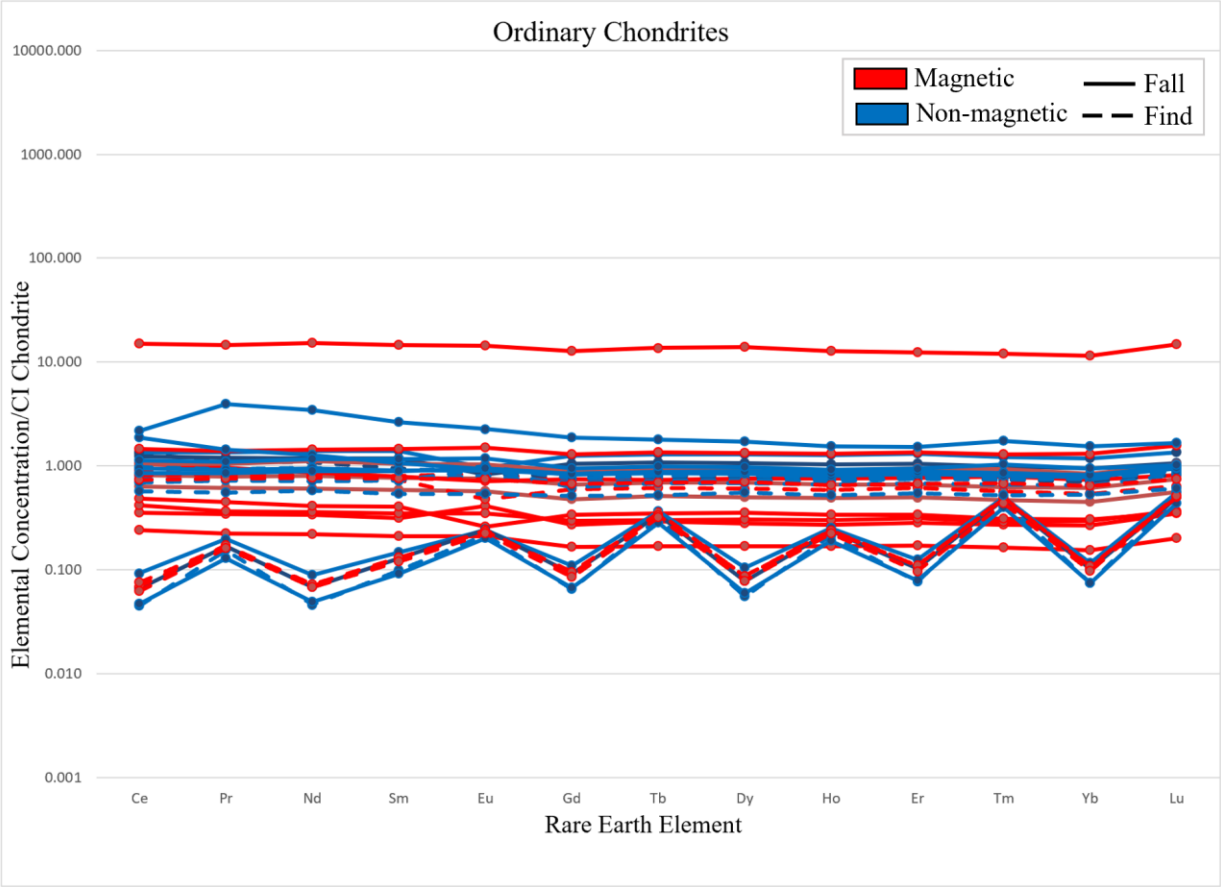

Figure 8. Chondrite normalized REE values for ordinary chondrites. Red and blue lines indicate the concentrations were measured on the magnetic and the non-magnetic fraction, respectively, of the samples. Solid lines are falls and dashed lines are finds.

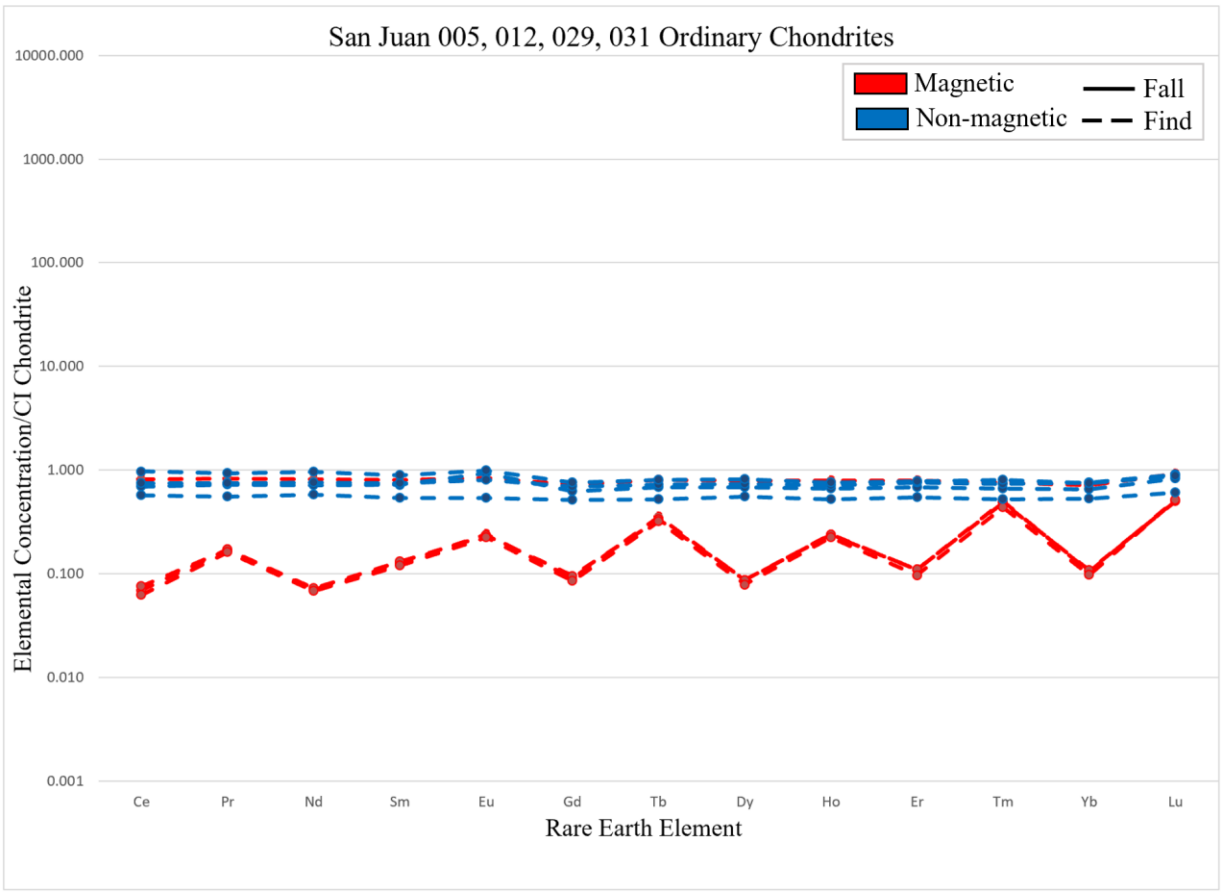

Figure 9. Chondrite normalized REE values for a select population of chondrite samples harvested from the San Juan meteorite field in Chile. Red and blue lines indicate the concentrations were measured on the magnetic and the non-magnetic fraction, respectively, of the samples. Solid lines are falls and dashed lines are finds.

ii. Carbonaceous vs. Ordinary

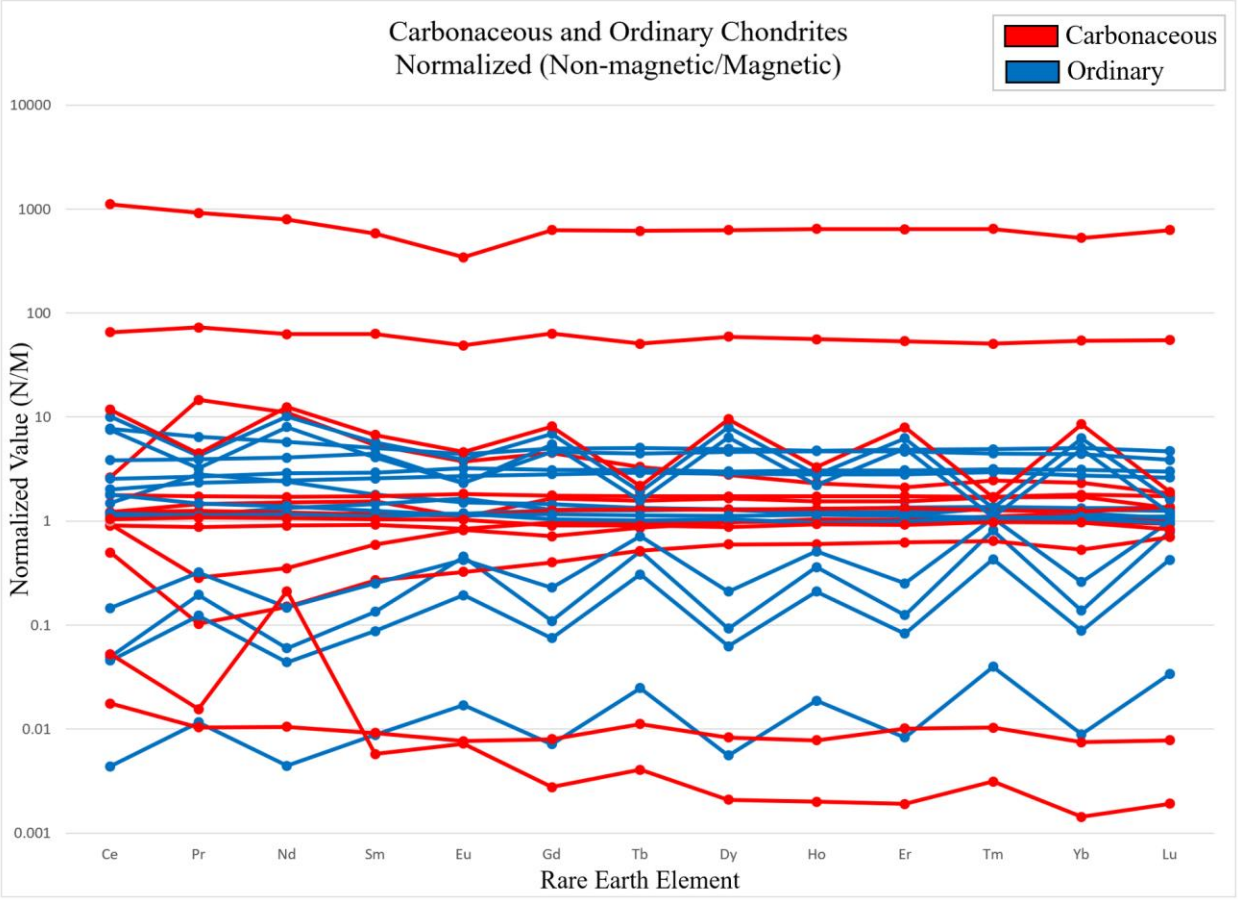

Figure 10. REE values of the non-magnetic vs. the magnetic fraction of carbonaceous (red) and ordinary (blue) chondrites.

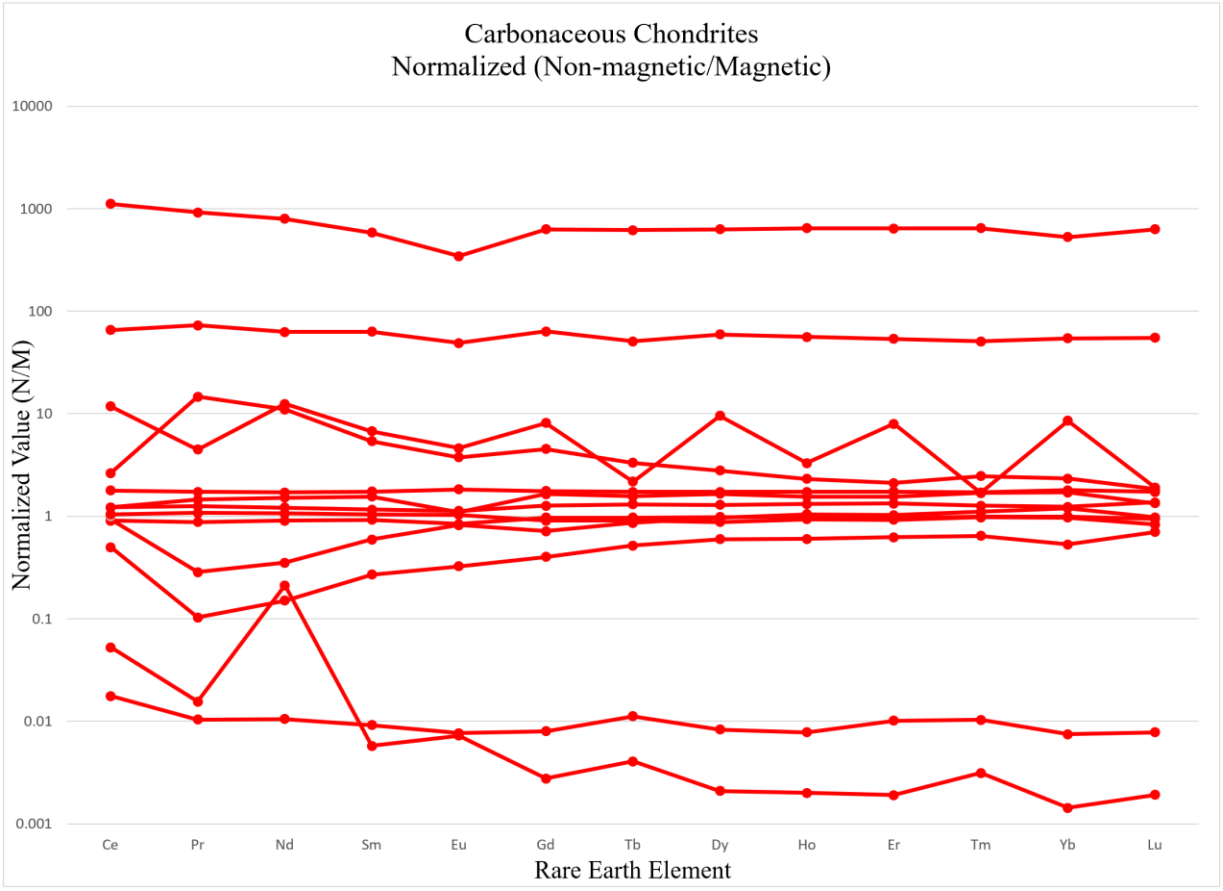

Figure 11. REE values of the non-magnetic vs. the magnetic fraction of carbonaceous chondrites. A chondrite more heavily enriched in an element in the non-magnetic mineral phase will plot higher on the graph, while a chondrite that is more enriched in a certain REE within the metallic mineral phase will plot lower on the graph.

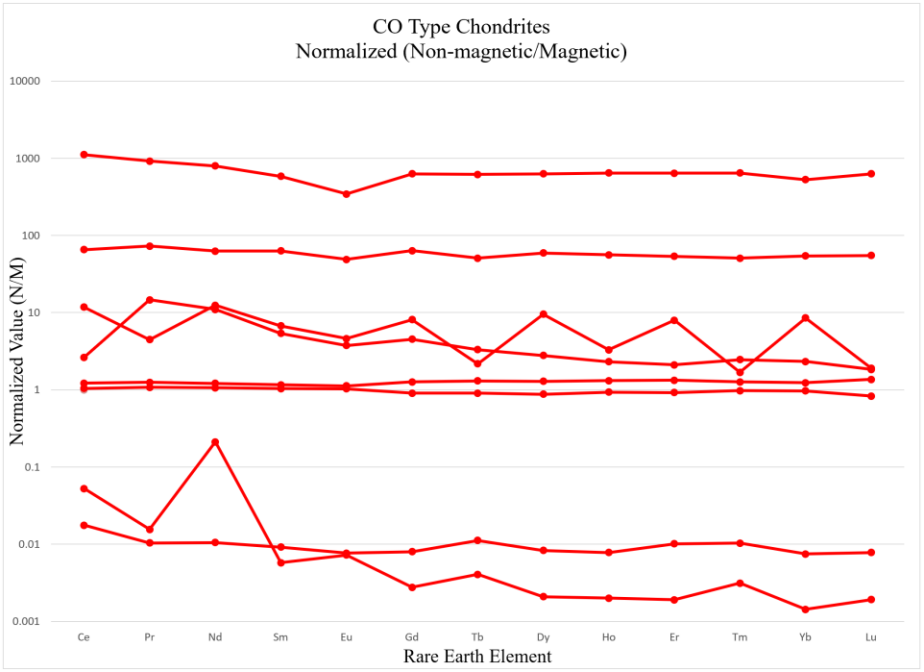

Figure 12. REE values of the non-magnetic vs. the magnetic fraction of CO type carbonaceous chondrites.

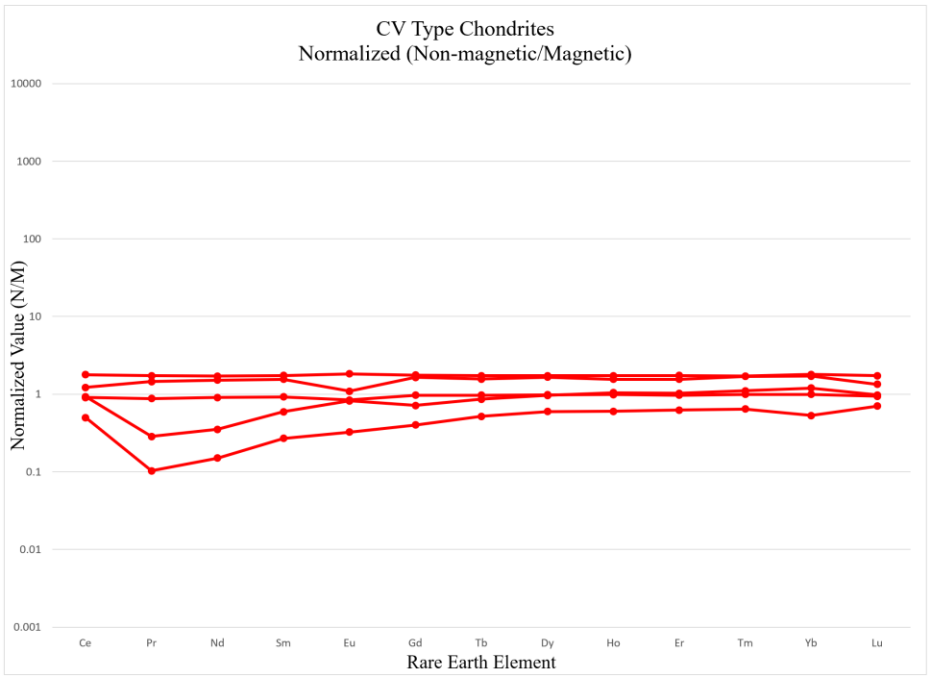

Figure 13. REE values of the non-magnetic vs. the magnetic fraction of CV type carbonaceous chondrites.

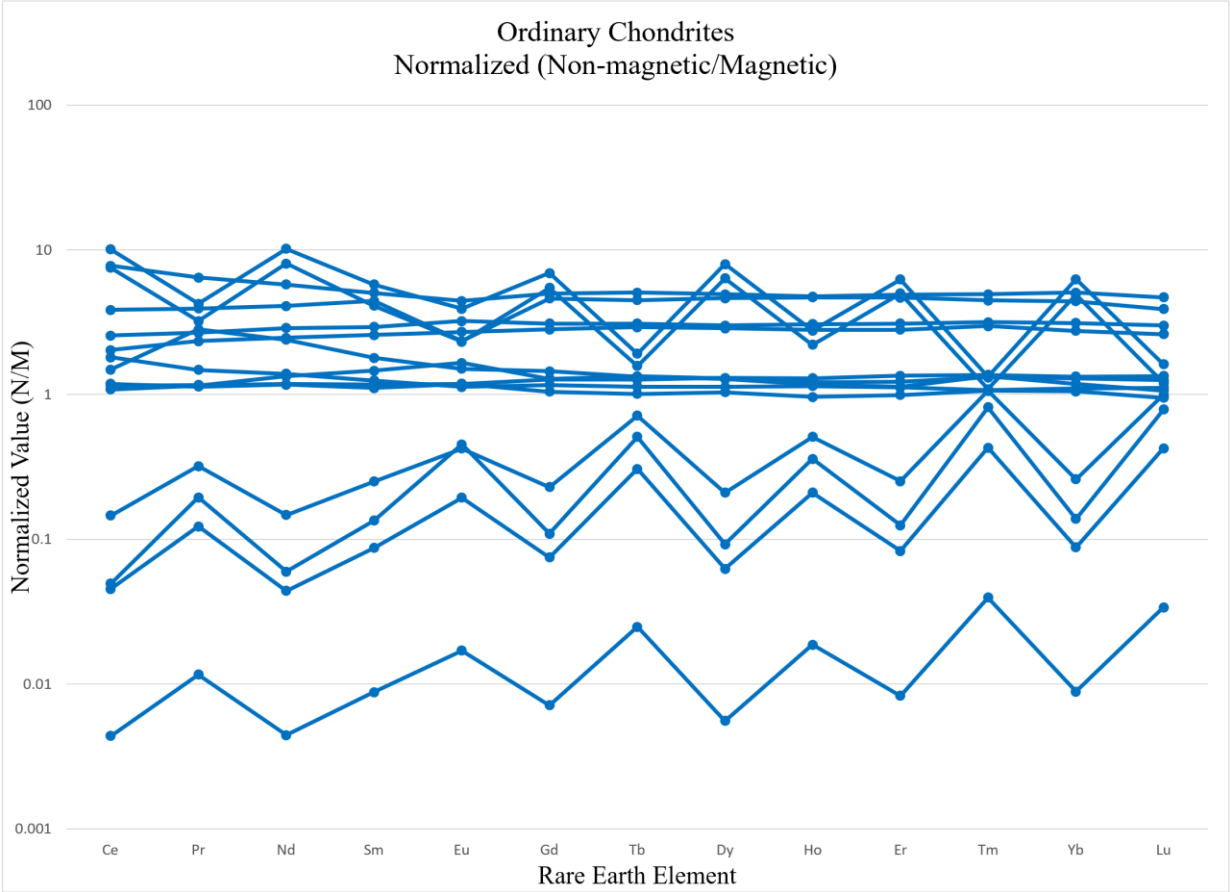

Figure 14. REE values of the non-magnetic vs. the magnetic fraction of ordinary chondrites. A chondrite more heavily enriched in an element in the non-magnetic mineral phase will plot higher on the graph, while a chondrite that is more enriched in a certain REE within the metallic mineral phase will plot lower on the graph.

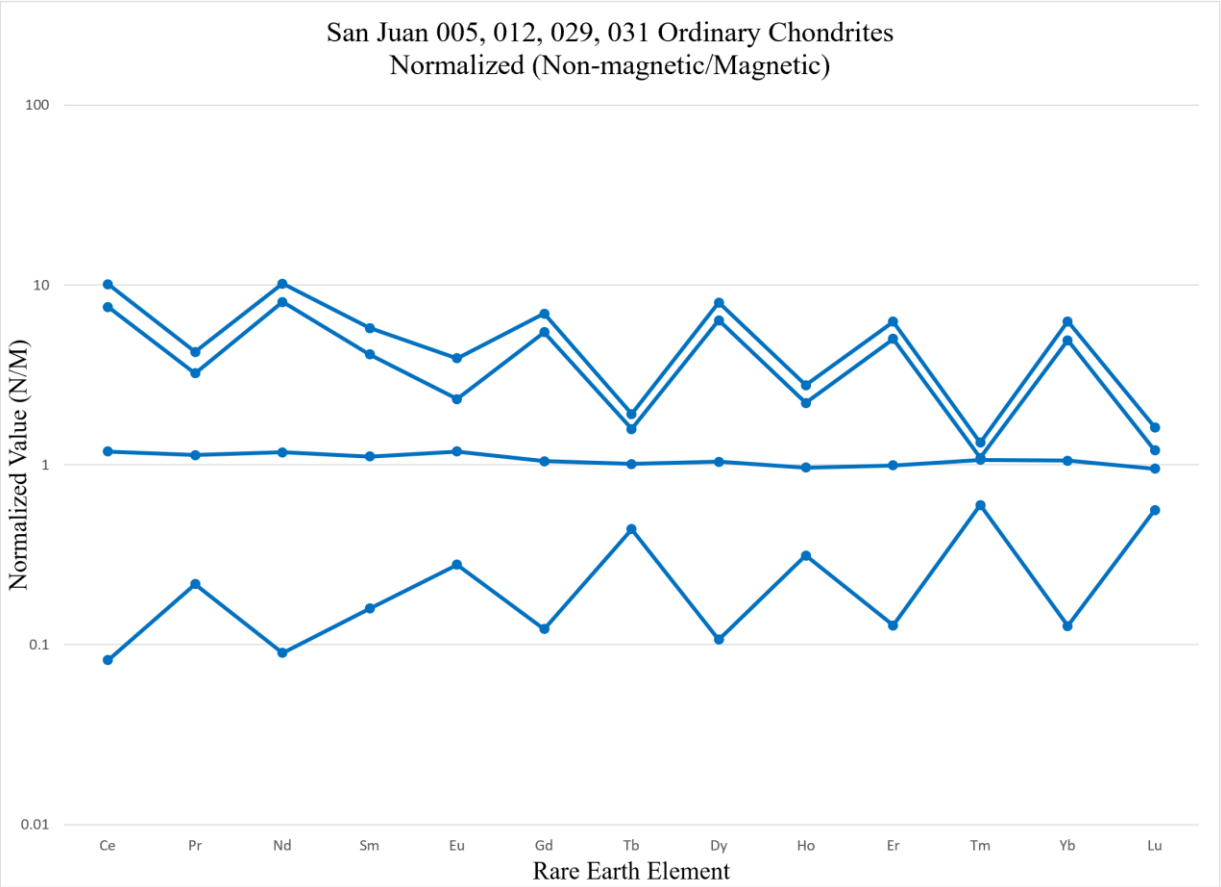

Figure 15. REE values of the non-magnetic vs. the magnetic fraction from the Chilean San Juan meteorite field.

iii. Falls vs. Finds

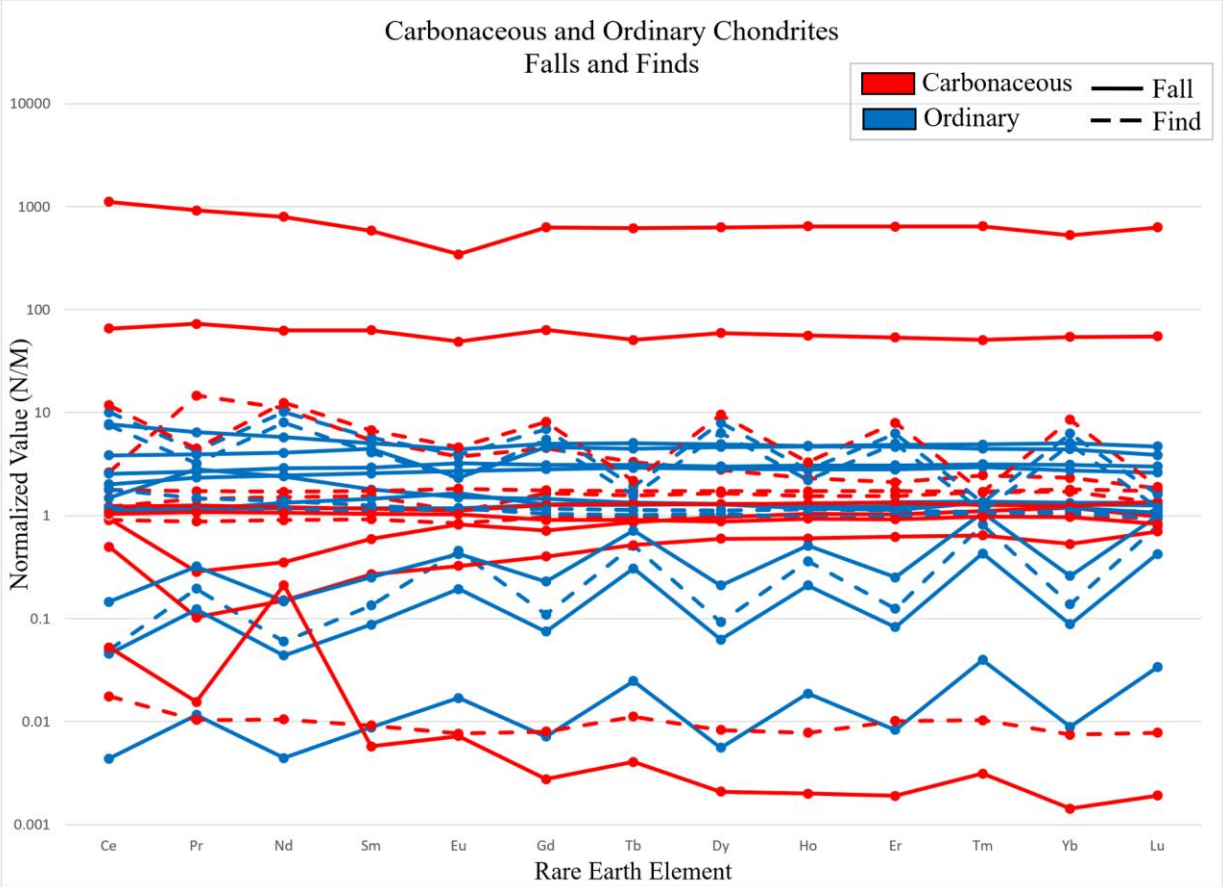

Figure 16. REE values of the non-magnetic vs. the magnetic fraction of carbonaceous (red) and ordinary (blue) chondrites. Solid lines indicate falls and dashed lines indicate finds. A chondrite more heavily enriched in an element in the non-magnetic mineral phase will plot higher on the graph, while a chondrite that is more enriched in a certain REE within the metallic mineral phase will plot lower on the graph.

a. Carbonaceous Chondrites

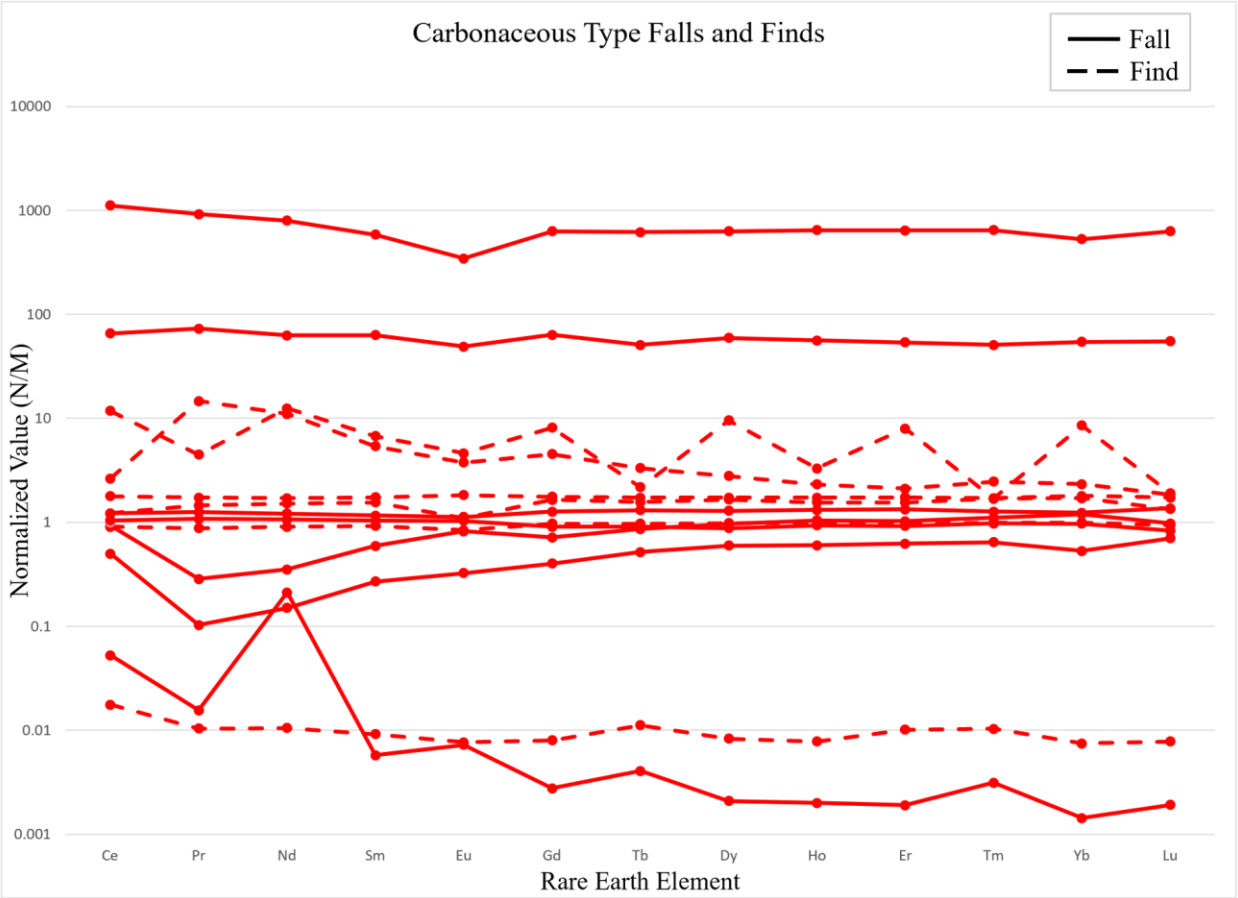

Figure 17. REE values of the non-magnetic vs. the magnetic fraction of carbonaceous chondrites. Solid lines indicate falls and dashed lines indicate finds A chondrite more heavily enriched in an element in the non-magnetic mineral phase will plot higher on the graph, while a chondrite that is more enriched in a certain REE within the metallic mineral phase will plot lower on the graph.

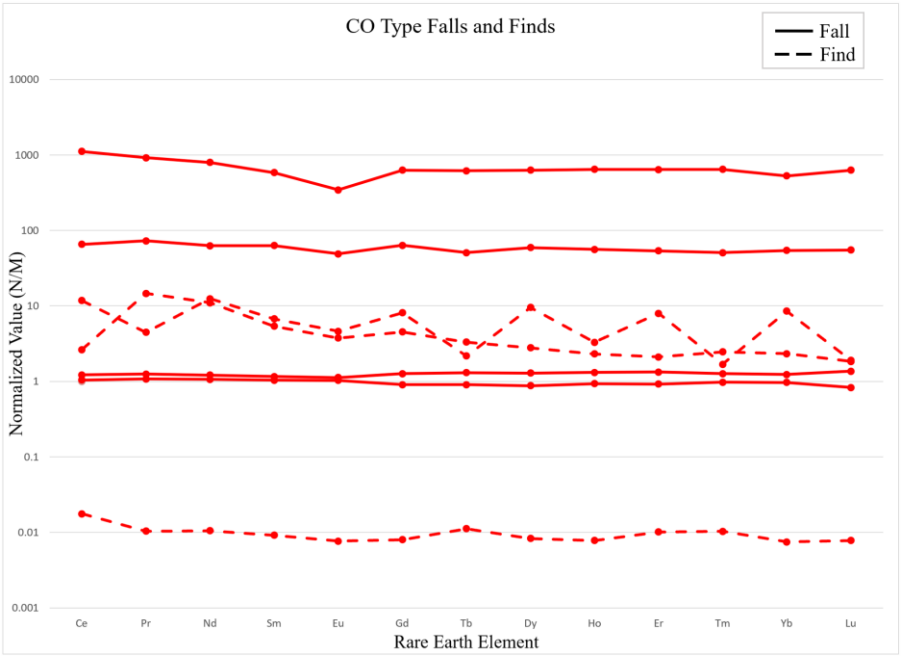

Figures 18. REE values of the non-magnetic vs. the magnetic fraction of CO type carbonaceous chondrites. Solid lines indicate falls and dashed lines indicate finds.

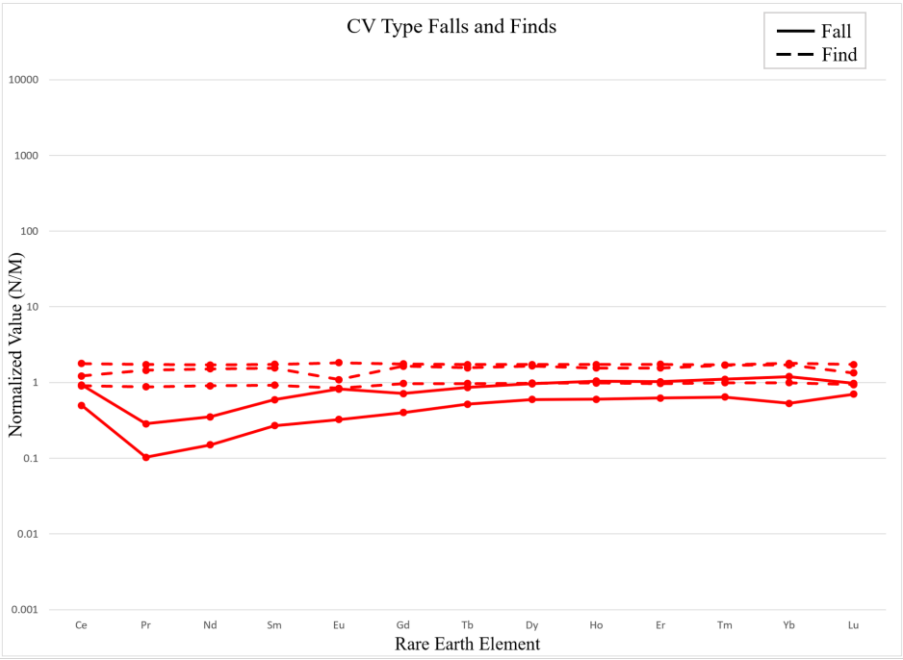

Figure 19. REE values of the non-magnetic vs. the magnetic fraction of CV type carbonaceous chondrites. Solid lines indicate falls and dashed lines indicate finds.

b. Ordinary Chondrites

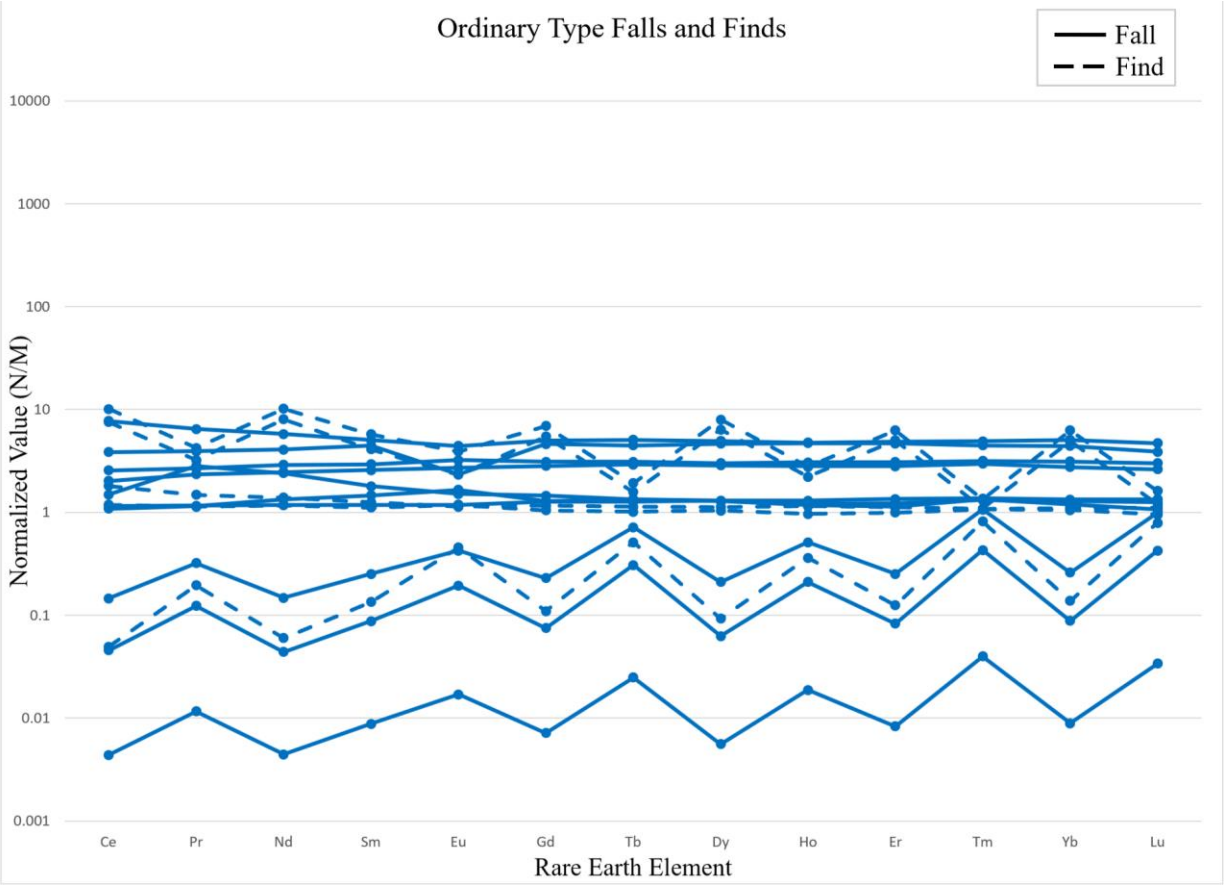

Figure 20. REE values of the non-magnetic vs. the magnetic fraction of ordinary chondrites. Solid lines indicate falls and dashed lines indicate finds.

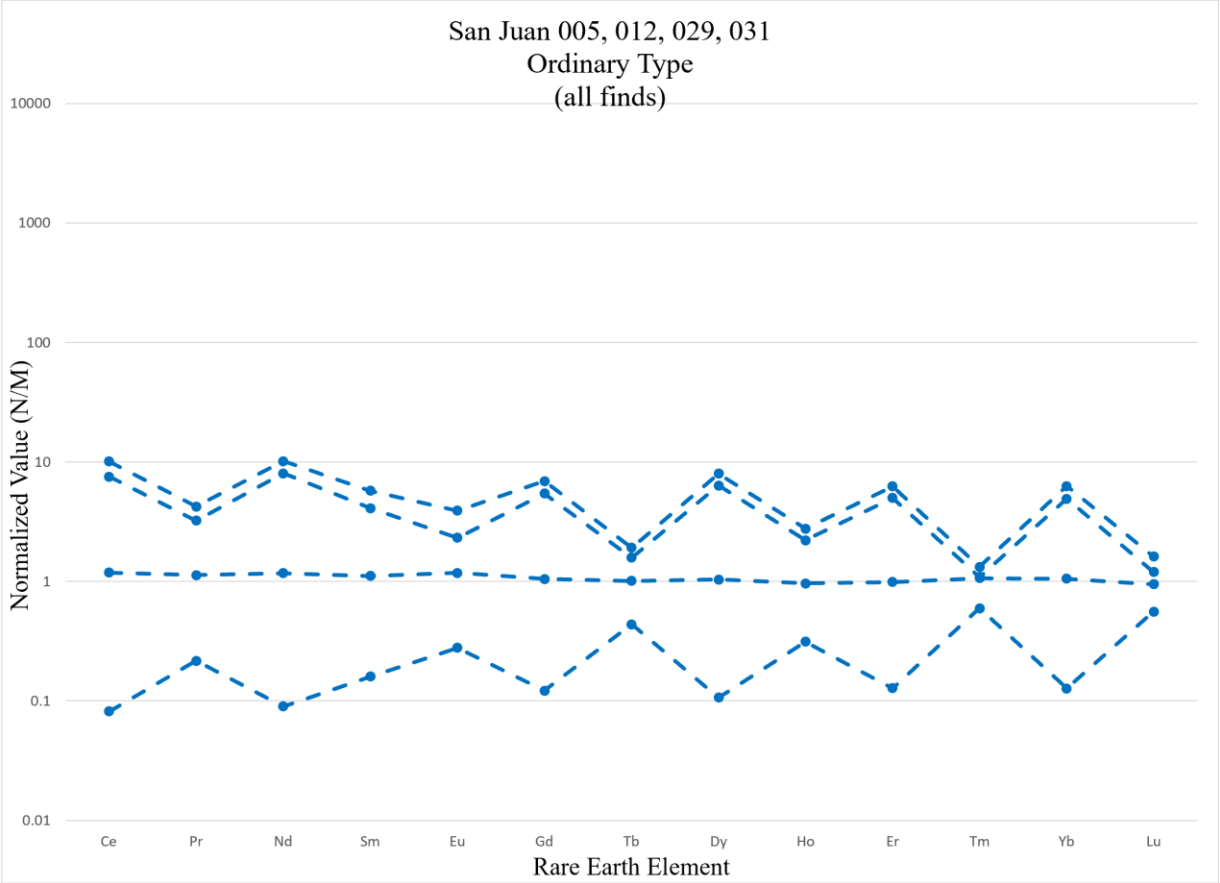

Figure 21. REE values of the non-magnetic vs. the magnetic fraction of the Chilean San Juan meteorite field. All ordinary chondrite samples from this location that were examined in this study were finds (dashed line).

Interpretation

i. Magnetic vs Non-magnetic

No obvious anomalous trends were identified throughout this exhaustive display of data. Most of the figures display a sawtooth shaped pattern spanning the entirety of the REE suite. One interpretation of this pattern is that it represents an accurate trend and that each sample examined in this study has differing levels of enrichment or depletion. However, this is unlikely since many REE studies have been performed on bulk composition of chondrite material and none have yielded such pattern. The CV subtype contained very little variance in concentrations

relative to CI (Figure 7) between the magnetic and non-magnetic mineral fractions. Two data series within the CV subtype displayed as magnetic falls (solid red line) exhibit 10-fold enrichments in Pr and Nd relative to CI.

When examining the ordinary chondrite group results in terms of magnetic and non-magnetic fractions, no clear separation of mineral phases is present (Figure 8). One data series, a magnetic fall, shows 10-fold enrichment relative to CI. A grouping of six data series comprised of magnetic and non-magnetic phases, both falls and finds, shows near-identical sawtooth patterns across the REE suite. The trend displays concentrations equivalent to a 10-fold depletion in REE relative to CI, with slightly less depleted values toward the less incompatible elements Tm and Lu.

Four ordinary chondrites in this study were all harvested from the San Juan meteorite field in Chile (Figure 9). San Juan samples (n=8) were separated from the larger ordinary chondrite population to see if there is a pattern within the REE concentrations between magnetic and non-magnetic mineral phases. All non-magnetic phases, as well as one magnetic phase series, contain very similar REE trends and show only slight depletion relative to CI. Three out of the total four magnetic phases examined were roughly ten times more depleted in REE relative to CI composition, and show near-identical sawtooth pattern becoming less depleted in less incompatible elements.

ii. Carbonaceous vs. Ordinary

When interpreting the results on the basis of chondrite type (carbonaceous or ordinary), few patterns emerge (Figure 10). The concentration data obtained from both the magnetic and non-magnetic phases were normalized by dividing the non-magentic concentration by the

magnetic concentration and plotted for each REE. Thus, if a data series plots high on the graph, it is more enriched in a REE in the non-magnetic mineral phase of that meteorite than the magnetic phase. Conversely, chondrites containing magnetic mineral phases that are highly concentrated in REE will plot lower on the graph.

Normalized concentration results from all carbonaceous chondrites are displayed in Figure 11. No logical patterns emerge from the dataset. There are two data series that show chondrites with non-magnetic phases that are 1,000 and 100 times, respectively, more enriched in REE than their corresponding magentic phases. If the carbonaceous chondrite group is divided into the CO and CV subtypes, a difference in REE concentrations between the groups becomes visible. CO chondrites (Figure 12) show a wide range of concentrations when compared to the CV chondrites (Figure 13). CO chondrites may contain equal REE concentrations between the magnetic and non-magnetic phases. However, they may also contain non-magnetic phases 1,000 times more enriched or more depleted in REE relative to their complementary magnetic phase (Fig. 12). CV chondrites exhibit far less variance in REE concentrations between the magnetic and non-magnetic phases for each chondrite. The overarching trend displayed within the CV subtype shows magnetic phases possessing roughly the same REE concentration as the non-magnetic phase for the same chondrite. Two data series show a slight enrichment of Pr within the magnetic mineral phases, but that does not apply to all data series.

Ordinary chondrites were displayed in the same manner (Figure 14). One chondrite contained a magnetic phase that was 100 times more enriched in REE relative to the non-magnetic phase, but the majority of ordinary chondrites displayed REE enrichments/depletions between phases less than or equal to a factor of 10. Ordinary chondrites were found to have a far

less extreme range of enrichments between mineral phases of the same chondrite than carbonaceous chondrites.

The four San Juan ordinary chondrites are displayed in Figure 15. One chondrite contained relatively similar REE concentrations in both magnetic and non-magnetic phases, while the remaining three showed less than or equal to a 10-fold enrichment/depletion of REE between mineral phases.

iii. Falls vs. Finds

Figure 16 displays the results (both carbonaceous and ordinary) for each chondrite (normalized value = non-magnetic phase concentration/magnetic phase concentration) in terms of falls (solid) and finds (dashed). As a whole, there are no clear groupings of falls or finds. No pattern emerges from the entire group, as both fallen and found chondrites occupy the entire range of concentrations. The carbonaceous type falls and finds are shown in Figure 17. Falls occupy the most extreme enrichment/depletion patterns, although the majority of the results show roughly similar REE enrichment in both the magnetic and non-magnetic phases of the same chondrite. CO subtypes, once again, exhibit the widest range of relative enrichment/depletion within magnetic or non-magnetic mineral phases (Figure 18). One CO type fall shows a 1000-fold enrichment in the non-magnetic phase, while another shows a 100-fold enrichment. One CO-type find contains a magnetic mineral phase that is 100 times more enriched in REE than the non-magnetic phase. The CV sub-type (Figure 19) shows that all finds contain about the same REE concentration within both magnetic and non-magnetic mineral phases, while the only two falls are slightly depleted in Pr within the non-magnetic phases relative to the magnetic.

Within the ordinary chondrites group, there were no discernable patterns with respect to falls or finds (Figure 20). Most chondrites within this group contained equal concentration of REE within both magnetic and non-magnetic fractions. There was only one chondrite that could be considered an outlier, with a non-magnetic phase showing 100 times higher concentration of REE than the magnetic mineral phase. All other chondrites within this group showed REE enrichement/depletion within a factor of 10 between the magnetic and non-magnetic mineral phases regardless if it was classified as a fall or find. The same pattern was identified within the San Juan ordinary chondrites, which are all classified as finds (Figure 21).

III. SULFUR ISOTOPE STUDY

Methodology

Chondrites (n=24) were examined in this study. Samples were crushed into particles roughly 1 mm in diameter and separated into magnetic and non-magnetic mineral phases using a magnet. A microbalance was used to measure a target weight of 0.4 mg of both silicate and metallic fractions of each sample, which were then packaged into tin capsules in preparation for combustion.

Table 6. The table below shows how many of each type of chondrite were included in the sulfur isotope study. Modified from White, 2013.

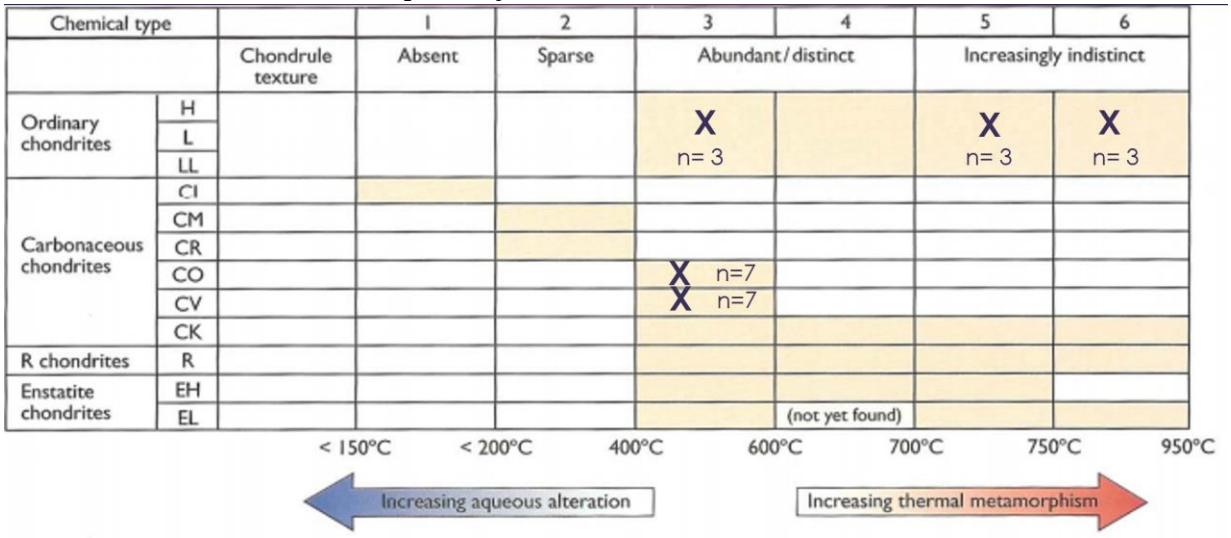

The samples were run on a Thermo Scientific (Bremen, Germany) EA Isolink system. The system includes an elemental analyzer equipped with a ramped GC oven interfaced with ConFlo IV to a Delta V Advantage Plus mass spectrometer. The samples were combusted at 1040℃ with the addition of an oxygen pulse. The resulting raw data was normalized using three standards: sulfanilamide (organic S), IAEA S-3 (silver sulfate, Ag_2SO_4), NBS-127 (barium sulfide, BaS) with average $\delta^{34}S$ values of -10.34, -32.30, and 20.30, respectively. The experimental data were reported with values for the $\delta^{34}S$ and percent sulfur content for both magnetic and non-magnetic phases for each of the samples. The data were imported into Jupyter Notebook and data analysis was performed using the Python 3.0 language and Microsoft Excel. The results showing the sulfur isotope values are found in Table 7.

Table 7. Results from the S experiment are listed above. They are categorized by chondrite name, type, magnetism, S signature, and percent S.

Chondrite	Type	Mag/Nonmag	$\delta^{34}S$	% S
Arch	CV	M	3.4964	0.9957
		N	0.2155	0.5593
Bali	CV	M	-0.3584	2.8239
		N	0.0205	2.1677
Bovedy	O	M	-0.0659	1.7841
		N	0.2870	1.5997
Chiang Khan	O	M	1.1951	0.5795
		N	1.3183	2.1909
Colony	CO	M	5.4494	0.9075
		N	4.2194	0.9147
Coolidge	CV	M	1.9451	1.1790
		N	3.1610	0.9599
Efremovka	CV	M	-0.0004	1.9637
		N	-0.4962	1.9539
Felix	CO	M	0.2158	2.1481
		N	3.2510	4.2888
Gheriat 002	O	M	1.4320	1.2611
		N	0.2589	1.8500
Isna	CO	M	0.1339	2.4490
		N	1.4754	1.2433
Jilin	O	M	1.7420	1.1964
		N	-0.2730	2.1302
Kaba	CV	M	-0.3442	2.2792
		N	-0.3218	2.0928
Kainsaz	CO	M	0.4429	2.1506
		N	0.1798	1.8840
Lance	CO	M	0.4462	1.9548
		N	0.6814	1.5440
Leoville	CV	M	-0.2176	1.9577
		N	2.0041	1.0218
Ornans	CO	M	0.6306	2.7031
		N	0.9262	2.0143
Renazzo	CR	M	-1.0025	0.9447
		N	0.2784	1.2775
San Juan 005	O	M	0.4942	2.2389
		N	-0.5016	1.9859
San Juan 009	CO	M	2.1743	0.8589
		N	0.1267	1.2228
San Juan 012	O	M	0.4516	1.9884
		N	-0.7475	2.3281
San Juan 029	O	M	0.9505	1.7777
		N	-0.6121	2.2503
San Juan 031	O	M	0.1263	2.1734
		N	-0.7713	2.0687
Sinawan 001	O	M	-0.5113	2.1147
		N	-0.2470	2.1697
Warrenton	CO	M	0.5990	1.7771
		N	0.1137	2.4033

i. Magnetic vs. Non-magnetic

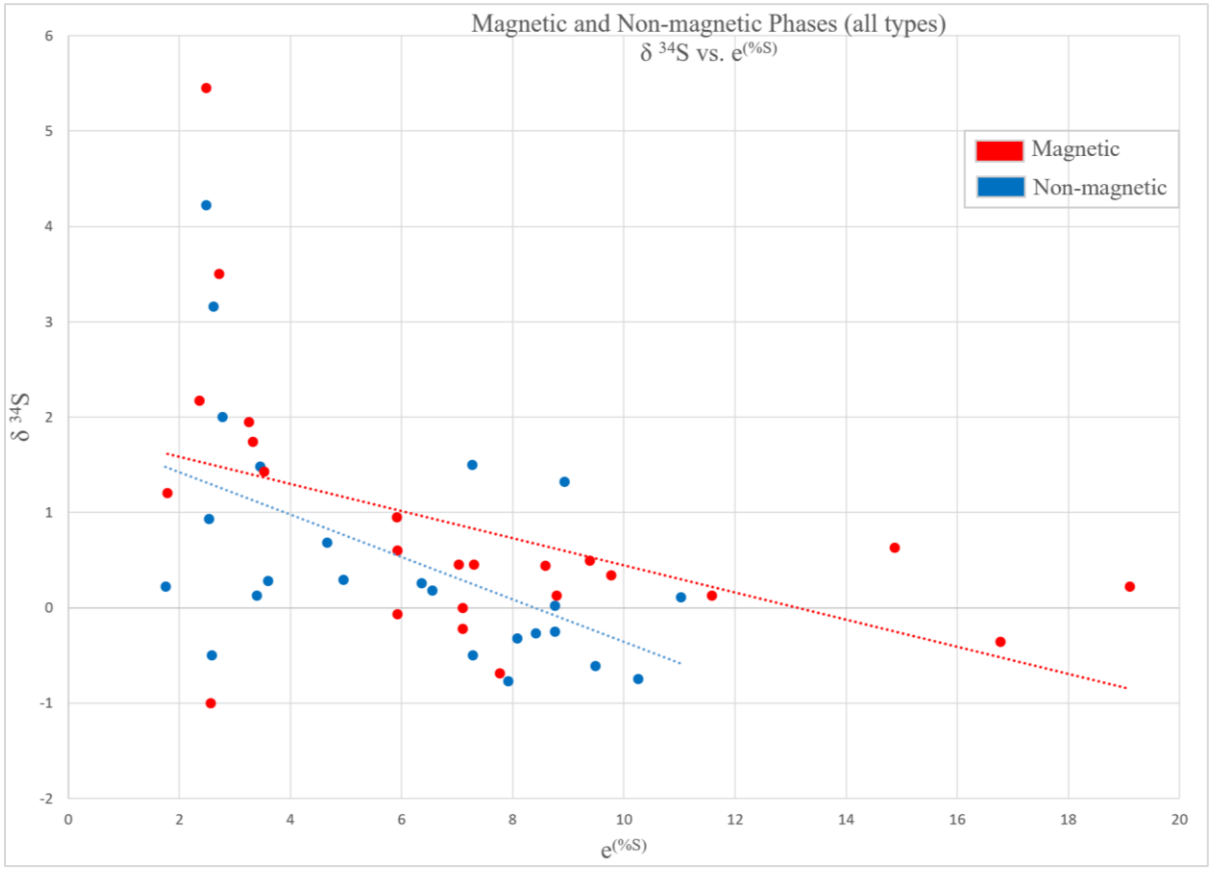

Figure 21. $\delta^{34}S$ versus $e^{(\%S)}$ values in all analyzed meteorite samples. Red symbols represent magnetic fractions and blue symbols represent non-magnetic fractions.

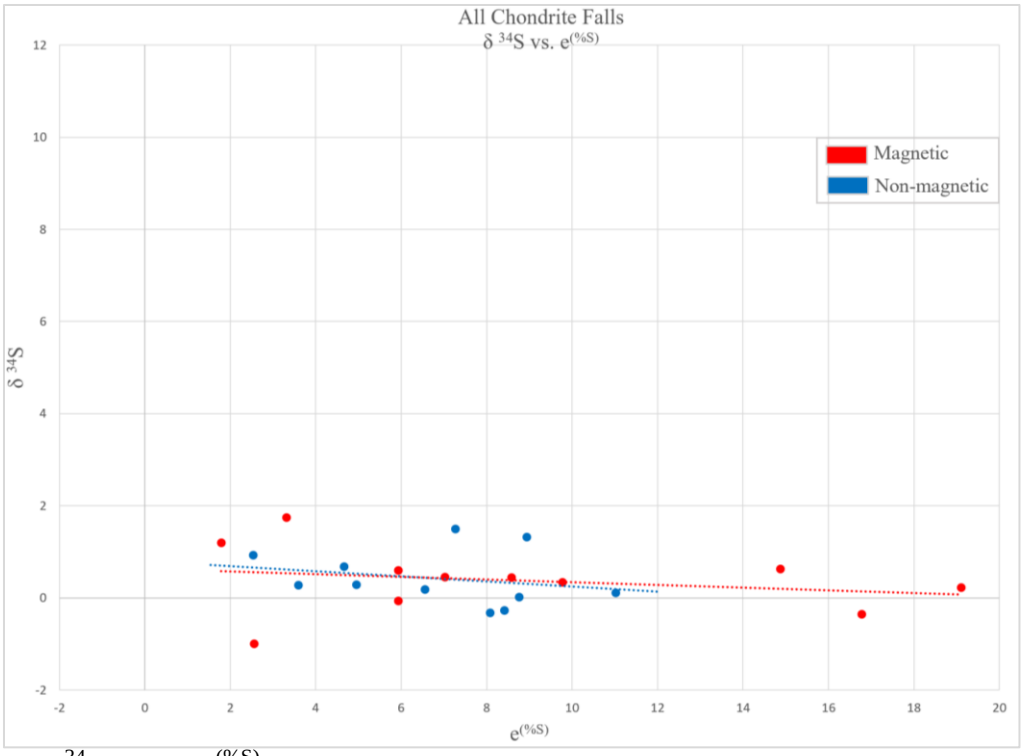

Figure 22. $\delta^{34}S$ versus $e^{(\%S)}$ values in all analyzed chondrite falls show little variance between non-magnetic and magnetic mineral phases present in the chondrites.

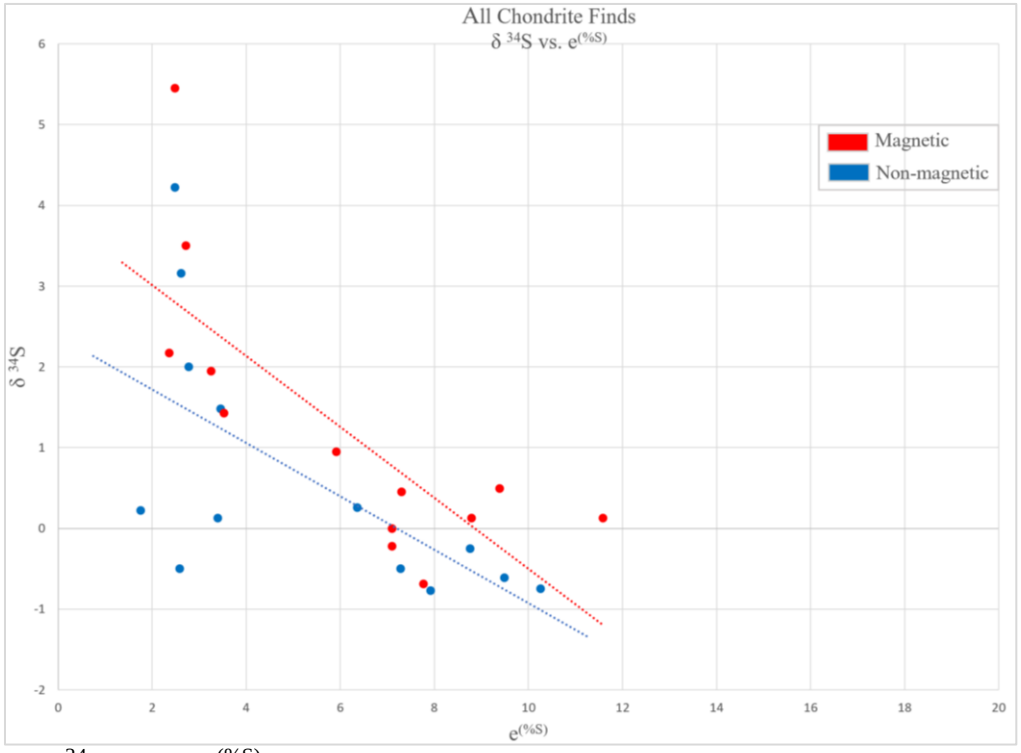

Figures 23**.** $\delta^{34}S$ versus $e^{(\%S)}$ values in all analyzed chondrite finds show little variance between non-magnetic and magnetic mineral phases present in the chondrites.

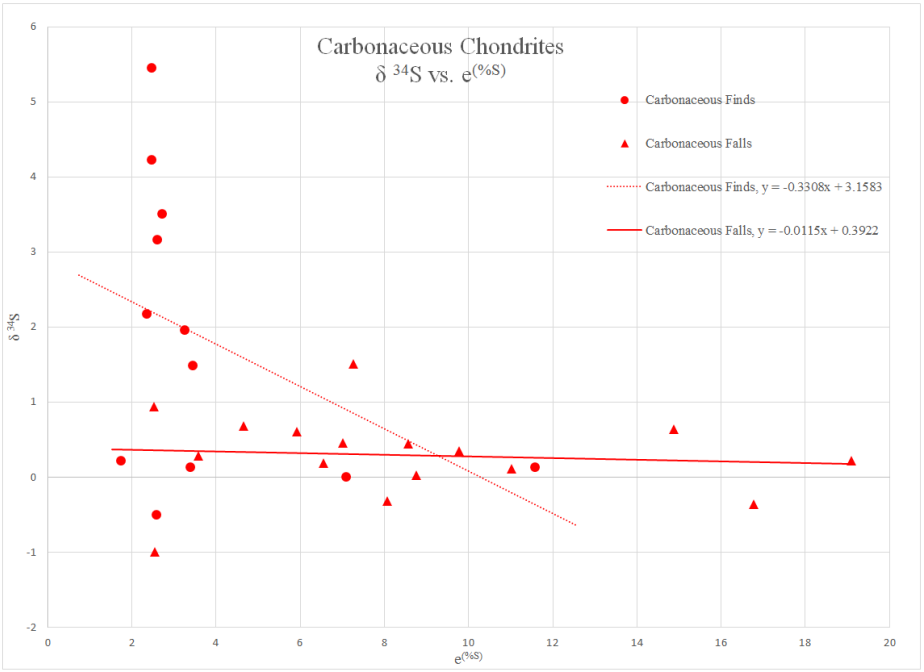

Figure 24. $\delta^{34}S$ versus $e^{(\%S)}$ values in all analyzed carbonaceous chondrites show similar patterns when comparing trend lines of falls and finds with all ordinary (Figure 25). Finds display a steeper trendline and less overall S content in both cases.

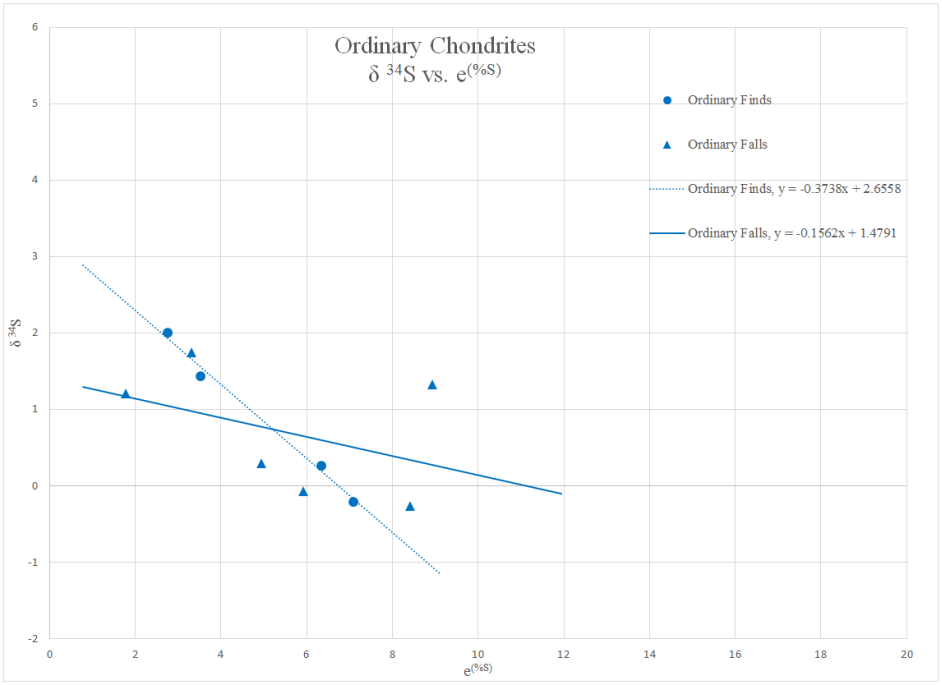

Figure 25. $\delta^{34}S$ versus $e^{(\%S)}$ values in all analyzed ordinary chondrites show similar patterns when comparing trend lines of falls and finds with all carbonaceous (Figure 24). Finds display a steeper trendline and less overall S content.

ii. Carbonaceous vs. Ordinary

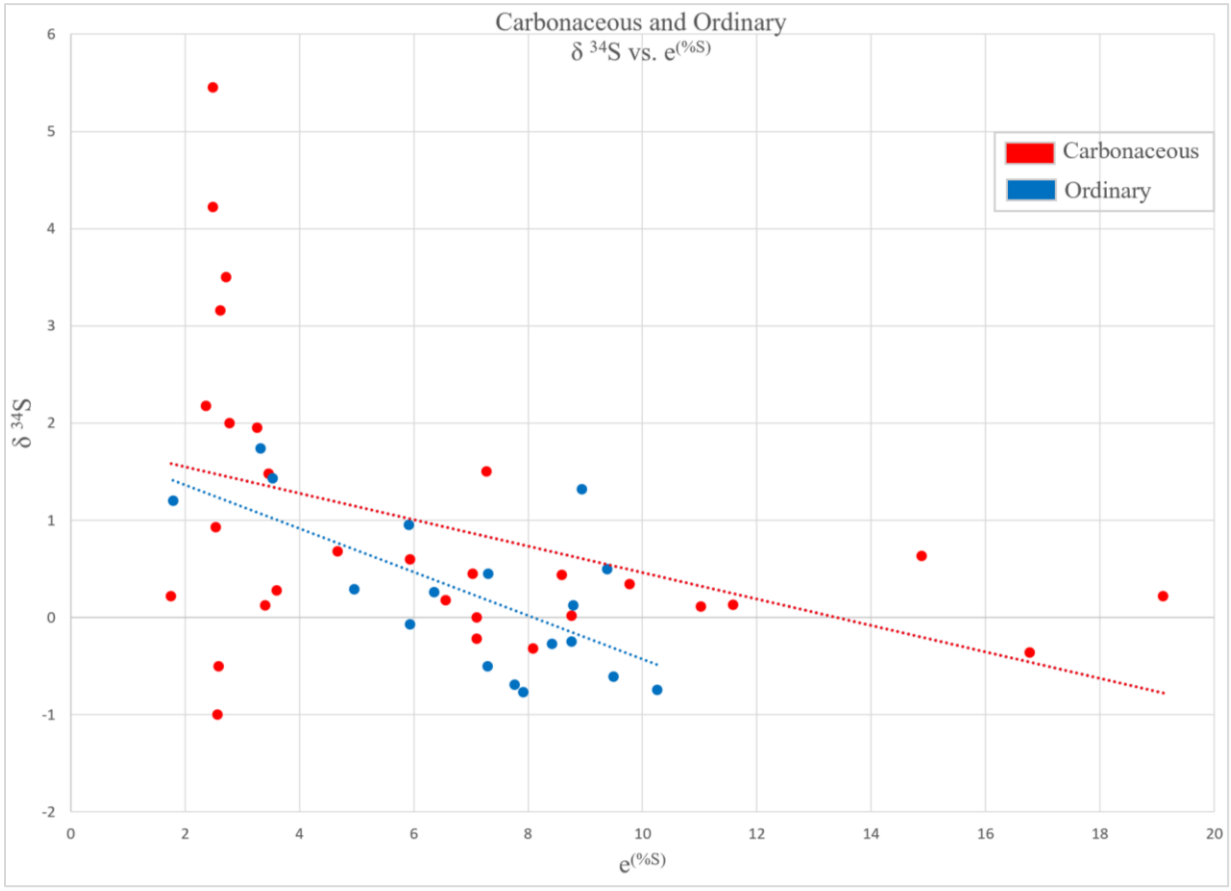

Figure 26. $\delta^{34}S$ versus $e^{(\%S)}$ values for all analyzed chondrites. Red symbols represent carbonaceous type and blue symbols represent ordinary type.

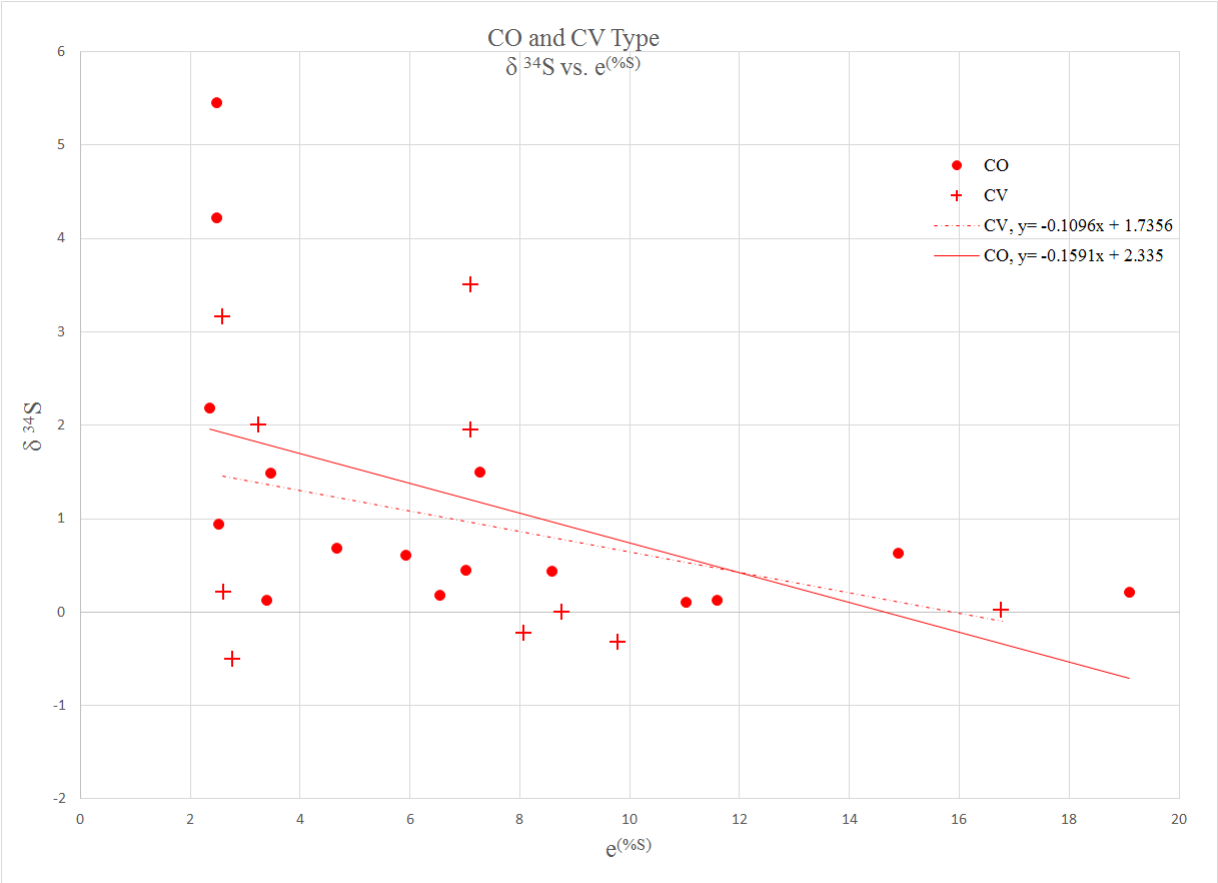

Figure 27. $\delta^{34}S$ versus $e^{(\%S)}$ values for all analyzed carbonaceous chondrites. CO type is represented by a closed circle and CV type is represented by a cross.

iii. Falls vs. Finds

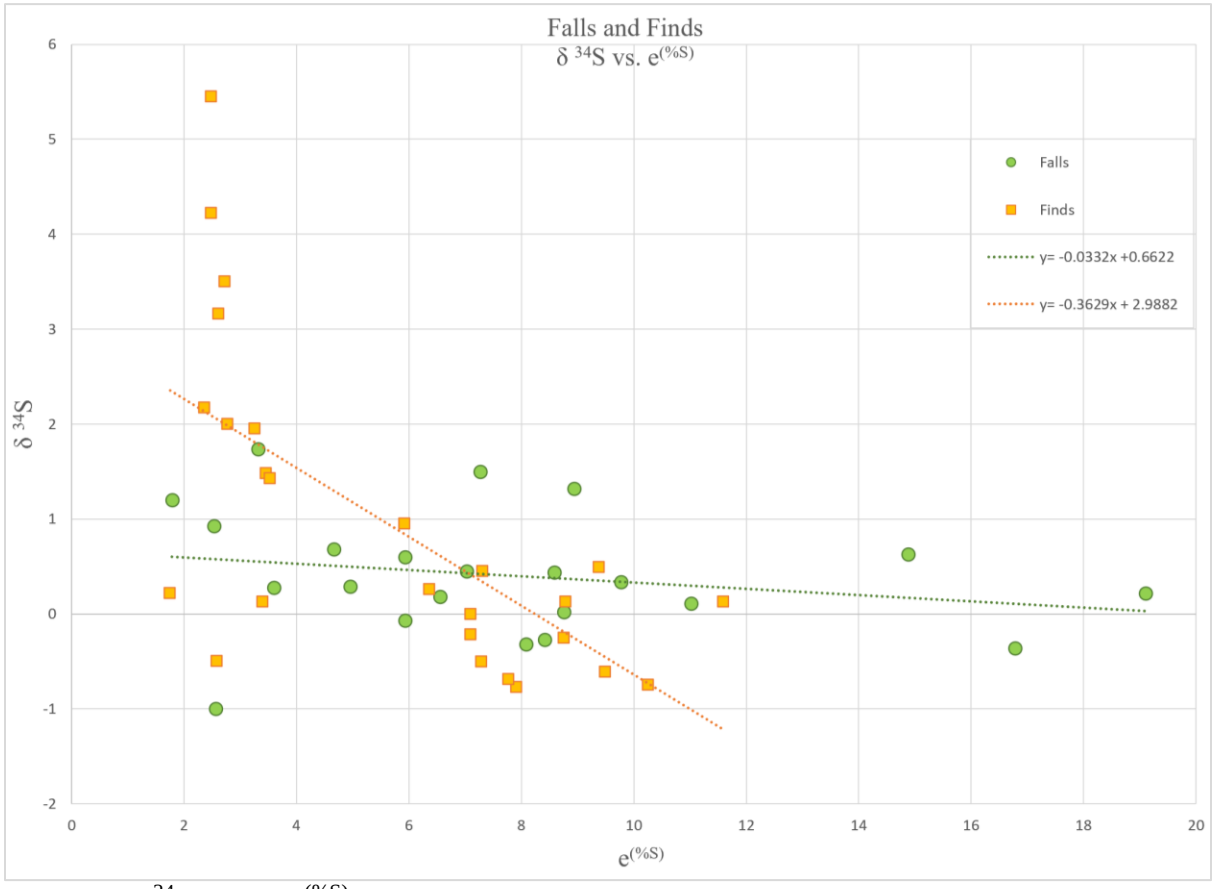

Figure 28. $\delta^{34}S$ versus $e^{(\%S)}$ values for all analyzed falls and finds, regardless of chondrite type. The difference in the slopes of the best fit lines (trendlines) indicate there are differences in the chemical makeup of the chondrites based on time spent on the earth's surface.

Interpretation

In order to to tell which mechanism of fractionation (mixing or reaction) is occurring within the condrites, the data were plotted $\delta^{34}S$ versus $e^{(\%S)}$. When a natural log is used in conjunction with the S abundance, in this case %S, the shape that the data takes will reveal a broad sense of fractionation mechanism. If a mixing reaction were altering the $\delta^{34}S$, then the data would form a hyperbolic shape. If the $\delta^{34}S$ is being altered strictly from a straightforward dissolution or precipitation reaction, the data will form a linear function (Kendall and McDonnell). In the instance of this study, all data formed mostly linear shapes, indicating the

samples were influenced by a straightforward dissolution or precipitation reaction to be altered to their current state.

i. Magnetic vs. Non-magnetic

When comparing results of magnetic and non-magnetic fractions, regardless of chondrite type, no clear trends appear between them. Values of both $\delta^{34}S$ and $e^{(\%S)}$ of the magnetic (*y= -0.1335x + 1.8128*) and the non-magnetic (*y= -0.2034x +1.8868*) mineral phases are shown in Figure 21. There is little difference in the spread of $\delta^{34}S$ values in both mineral phases, though a wider range of sulfur content was present in the magnetic phase than the non-magnetic phase. This may be attributed to variable mineralogical makeup within the magnetic phases across the chondrite types, but is not substantial enough to state a clear pattern exists.

When examining magnetic and non-magnetic phases within all chondrite falls (Figure 22), the data are remarkably similar in their $\delta^{34}S$ signature, but highly variable in their S content. This means that even though the amount of S present varies, the S species are remarkably similar and have not experienced fractionation when exposed to earth's atmospheric conditions. Figure 23 displays the chondrite finds separated into magnetic and non-magnetic phases. Overall, both the magnetic and the non-magnetic phases within this group display similar results. Chondrite finds, when compared to the falls group in Figure 22, exhibit a far more diverse range of $\delta^{34}S$ values and a lower average S content. The wide range of $\delta^{34}S$ shows the chondrite finds have experienced fractionation within the earth's system. The lower S content displayed within the chondrite finds may also be due to mobilization of S due to alteration (weathering) processes.

The $\delta^{34}S$ signatures in magnetic and non-magnetic chondritic mineral phases are remarkably similar. This may be credited to the dual classification by Goldschmidt of sulfur's

behavior as both lithophile and chalcophile. The maximum value of S content in metallic mineral phases is greater than the maximum value within silicate mineral phases. The presence of higher S content values in metallic phases is explained by the fact that chondrites contain a higher percentage of metallic sulfur-bearing minerals than silicate sulfur-bearing minerals.

ii. Carbonaceous vs. Ordinary

Comparing the carbonaceous group to the ordinary group (Figure 26), the former varies widely in both $\delta^{34}S$ and $e^{(\%S)}$ values compared to the latter. Overall, the carbonaceous group varies more in both $\delta^{34}S$ and S content, possibly reaffirming the difference in microstructures between the two groups of chondrites. Carbonaceous falls (*y= -0.0115x +3.922*) exhibit a relatively uniform $\delta^{34}S$ values, but vary widely in S content (Figure 24). Carbonaceous finds (*y= -0.3308x + 3.1583*) exhibit a wide range of $\delta^{34}S$ values, but marginal variance of S content (Figure 24). Ordinary falls (*y= -0.1562x + 1.4791*) and ordinary finds (*y= -0.3738x + 2.6558*) plot in a narrower area (Figure 25) compared to the carbonaceous chondrites, with no significant differences. Upon further examination of the carbonaceous group by subtype (Figure 27), no differences appear to exist in $\delta^{34}S$ or S content. This may be due to the subtypes containing most similar microstructural characteristics when compared to the ordinary group as a whole.

Carbonaceous chondrites showed a wider spread of values in both isotopic signature and S content, which can act as signals for the response of the sample to its environment. Carbonaceous chondrites contain a lower percentage of chondrules and higher percentage of matrix material that make up the rock body, meaning more exposed surface area for interaction with reactants. This means the matrices of the carbonaceous group were more greatly affected by terrestrial weathering earlier in the terrestrial residency than their ordinary counterparts. Carbonaceous chondrites are also more enriched in volatile elements and contain an abundance

of organic compounds (Bland et al, 2006).

iii. Falls vs. Finds

The values of $\delta^{34}S$ versus $e^{(\%S)}$ were plotted for all falls and finds (Figure 28). Falls have a trendline of $y = -0.0335x + 0.642$. There is little variance in $\delta^{34}S$ values for falls, though the $e^{(\%S)}$ values vary considerably. Finds have a trendline of $y = -0.3813x + 3.2024$. There is a greater variation of $\delta^{34}S$ values for finds, however $e^{(\%S)}$ does not vary as much as within the falls.

It appears it is possible to determine a rough relationship between the $\delta^{34}S$ and the length of time a found meteorite has been residing in the field based on the S isotope signature present in the sample. At the very least, it is reasonable to assume the finds with a heavier $\delta^{34}S$ signature have been residing in situ longer than found meteorites with a relatively light $\delta^{34}S$ signature.

IV. DISCUSSION

REE Concentration Study

The sawtooth patterns exemplified throughout the entirety of the REE dataset can be attributed to the Oddo-Harkins Rule which states even-numbered elements are more abundant than the odd-numbered elements adjacent to them on the periodic table (Figure 29). This phenomenon can be explained as elements with odd atomic numbers have one unpaired proton, making them more likely to capture another, which increases their atomic number to an even one (Inglis-Arkell, 2015).

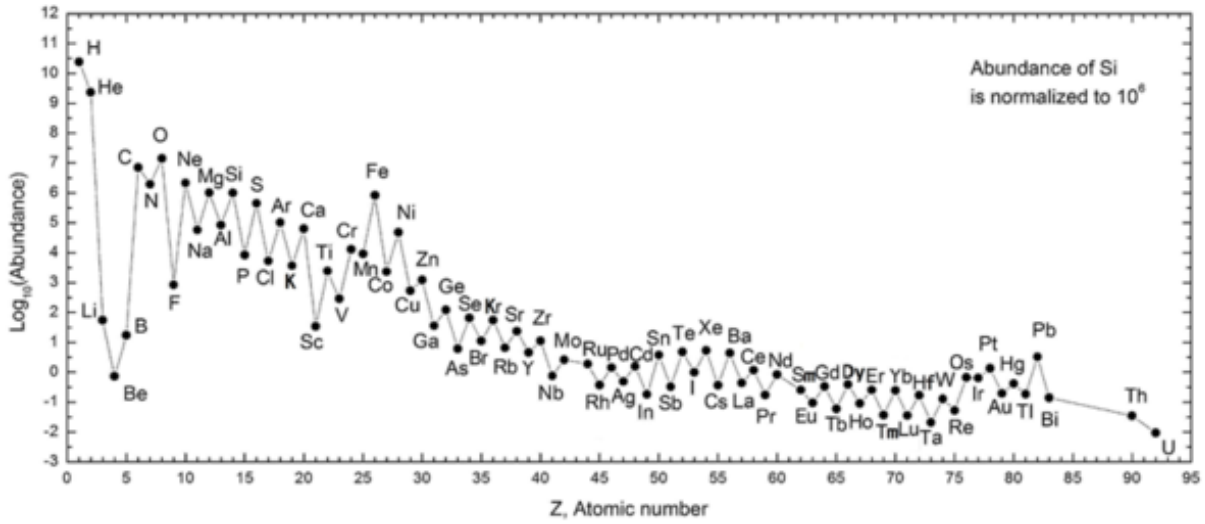

Figure 29. The elements of the periodic table exemplifying the sawtooth pattern explained by the Oddo-Harkins Rule, where even-numbered elements are more abundant than odd-numbered. (Modified from Inglis-Arkell, 2015)

This observational study determined REE values within the studied population to be reasonable. Anomalous quantities of a certain element may be attributed to the presence of a REE-bearing mineral, such as feldspars and pyroxenes (Bea, 2004), or be an indicator of formation conditions of the chondrite in question. For example, positive Thulium (Tm) anomalies are known to be indicative of material from the inner solar system formed from a reservoir of gas depleted in refractory dust (Dauphas and Tourmand, 2015). Positive Tm anomalies can be observed in select data series within Figures 5-21, mostly within ordinary chondrites. While this observation does not reveal much about the weathering patterns these select chondrites experience on Earth, it does provide reasoning for the enrichment/depletion patterns observed. Ordinary chondrites are more likely to exhibit a Tm anomaly due to the fact they have primitive asteroid parentage and were formed in what is now the inner solar system. Carbonaceous chondrites, by contrast, originate from ice-bearing rocky bodies further from the inner solar system (White, 2013).

Another such element with anomalous concentrations in select data series is Europium (Eu). Anomalous Eu concentrations are expected within the meteorites due to the distinct +2 valence and atomic radius, which create decoupling from the rest of the REE (Bea, 2004). The Eu anomaly is well-studied with respect to REE concentrations, and serves to verify the validity of the dataset.

Neodymium (Nd) anomalies are present within select data series in Figures 5-21. These Nd anomalies are not confined to a specific petrologic class, sub-type, or any other grouping. Neodymium is considered a 'light' REE and becomes concentrated in select mineral phases common in chondrites such as feldspars (Bea, 2004). It is not easily mobilized by water, and its concentration in natural waters is extremely low (Faure), implying observed concentrations of Nd are due to original mineralogy within the chondrite body and not from terrestrial alteration. Although a study of radioisotope systematics within these chondrites would need to be performed to substantiate this claim, one possible interpretation of the dataset is the chondrites bearing Nd anomalies have longer terrestrial residence times than those which do not, and instead contain the ^{147}Sm parent isotope.

The highly varied nature of the REE dataset is expected when attempting to consider many variables at once. The studied chondrite population vary not only in petrologic type, sub-type, terrestrial residence time, but also in mineral assemblages and environmental conditions of impact site. The aforementioned variables each play a role in the way a chondrite will interact with the terrestrial environment, and subsequently become weathered. The REE within these chondrites undergo fractionation, viewed here as enrichment/depletion trends, and leaching of dissolved fractions from rock by weathering.

Sulfur Study

Previous chondritic S studies (Monster et al., 1965; Kaplan and Hulston, 1966; Gao and Thiemens, 1993) separated the various sulfur components from chondrites and demonstrated that sulfides are characterized by the highest $\delta^{34}S$ values, whereas sulfates have the lowest $\delta^{34}S$ values. This happens to be the opposite from what is generally observed in terrestrial samples and is strong evidence against microbiological activity, implying instead a kinetic isotope fractionation in a sulfur–water reaction (Monster et al. 1965). Further evidence in support of a sulfur-water reaction as the main agent of fractionation in this case is the linear shape the $\delta^{34}S$ values take when plotted against the natural log of the S content, $e^{(\%S)}$, shown in Figures 21-28. If somehow a mixing were occurring, the data would plot hyperbolically, which is not the case.

The current data suggest S present within the chondrites is derived from a sulfate source, given the overall $\delta^{34}S$ is relatively low irrespective of class, magnetic predilection, or potential residence time. The presumed sulfate content is likely derived from mobilization of S by fluids from S-bearing minerals present in the chondritic body. The effects of presumed fluid presence at the impact site of each meteorite was further examined by plotting the impact locations on a global map displaying precipitation data using ArcGIS software (Figure 30). The basemap, although only displaying mean precipitation values from September 2000, serves well to illustrate the highly variable climatic conditions in which the chondrites were harvested.

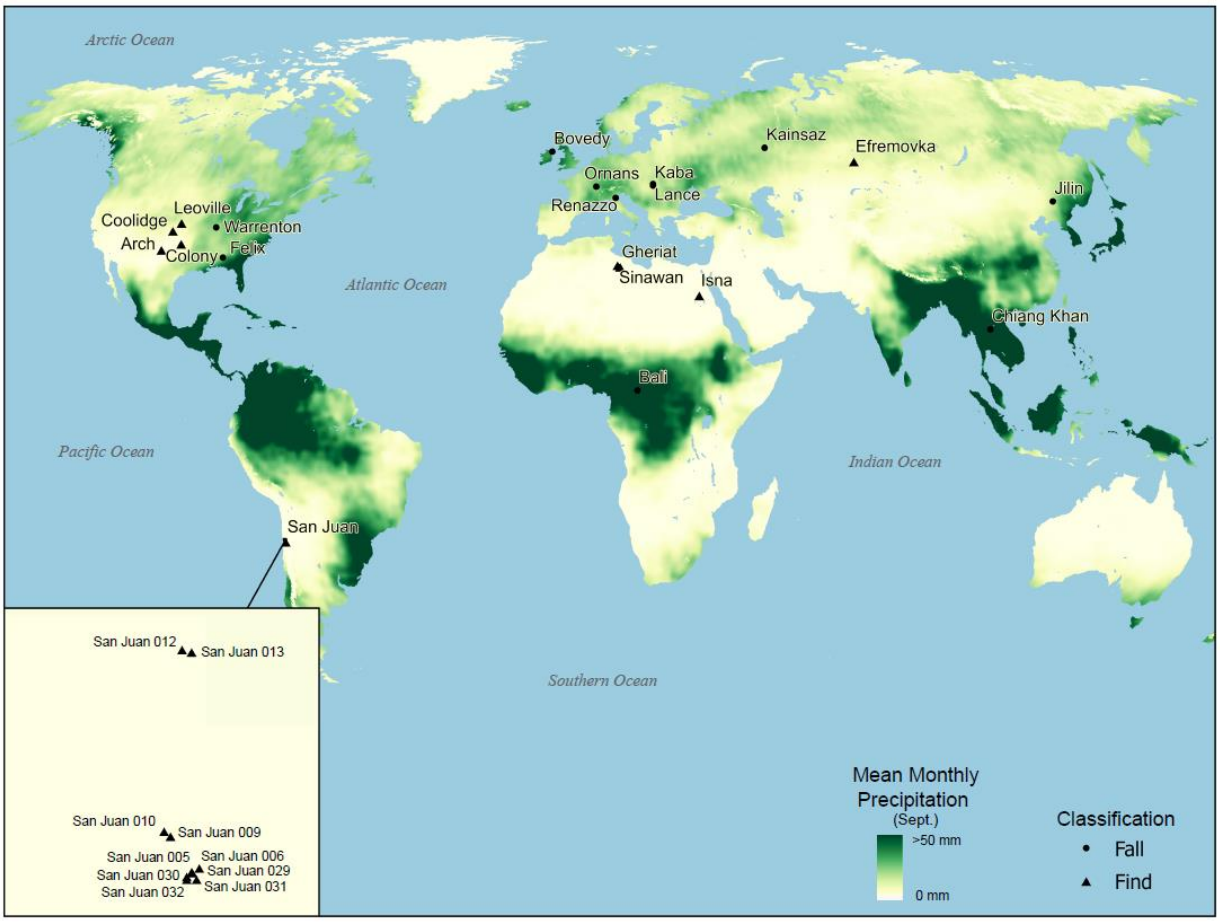

Figure 30. Global map including impact locations of all meteorites used in the S study. The basemap (GLDAS_Precipitation) shows the mean precipitation for the month of September in 2000.

When plotting $\delta^{34}S$ versus average annual precipitation (Figure 31) for all chondrites, few trends emerge from the data. One observation from this analysis is ordinary finds appear to fractionate heavier S species in places with increased precipitation. This misleading effect can be explained by the studied population being harvested from only impact sites with low amounts of annual precipitation; no ordinary finds from places of high annual precipitation were examined.

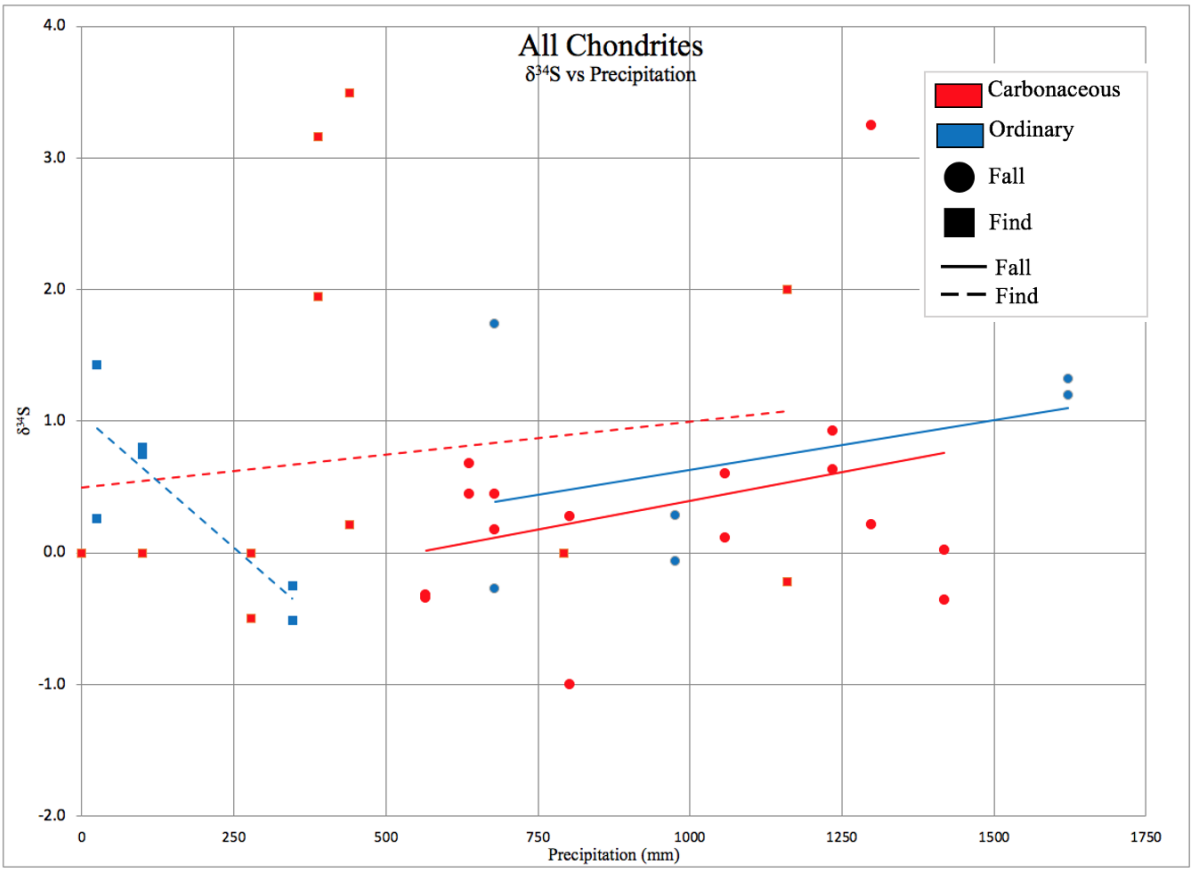

Figure 31. $\delta^{34}S$ versus precipitation values (in millimeters). Carbonaceous (red) and ordinary (blue) type chondrites are both displayed along with falls (circles) and finds (squares) within each group. No trend lines are displayed to avoid confusion within the figure.

Plotting precipitation values against $\delta^{34}S$ of falls and finds chondrites, no discernable difference between the two groups is noticed. Although determined $\delta^{34}S$ values within carbonaceous chondrites vary from -0.32‰ to 1.50‰, carbonaceous falls and finds display similar trendlines (Figures 32, 33). By comparison, ordinary falls and finds display very different trendline slopes which can be attributed to this study not including any ordindary finds from areas with high amounts of annual precipitation (Figures 32, 33).

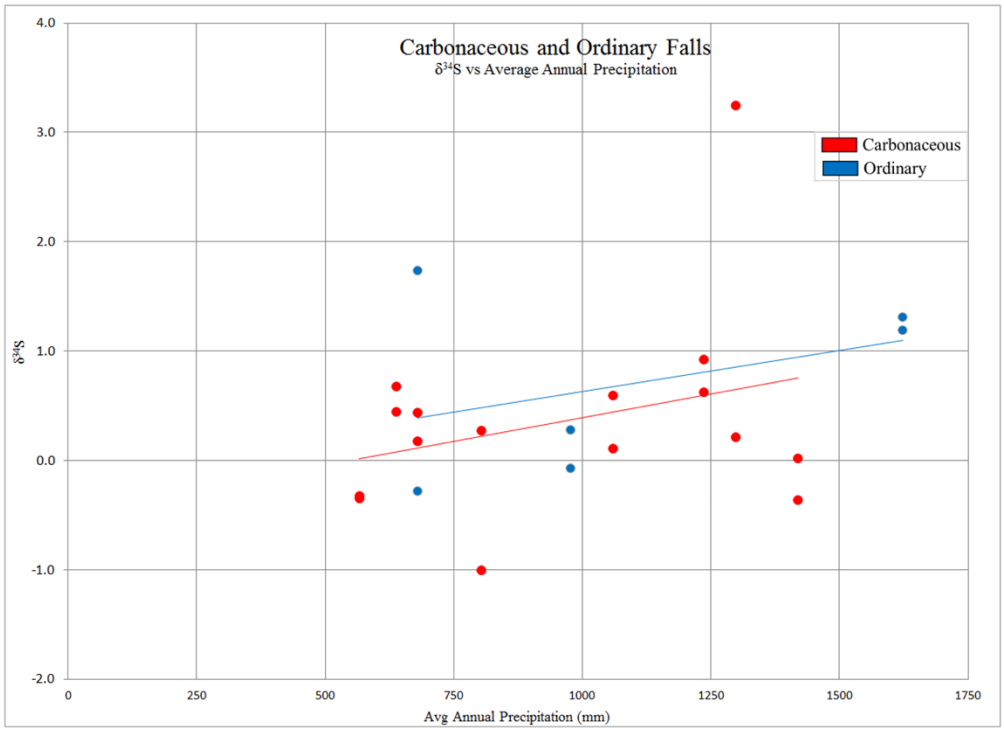

Figure 32. $\delta^{34}S$ versus average annual precipitation values (in millimeters) in all analyzed chondrite falls.

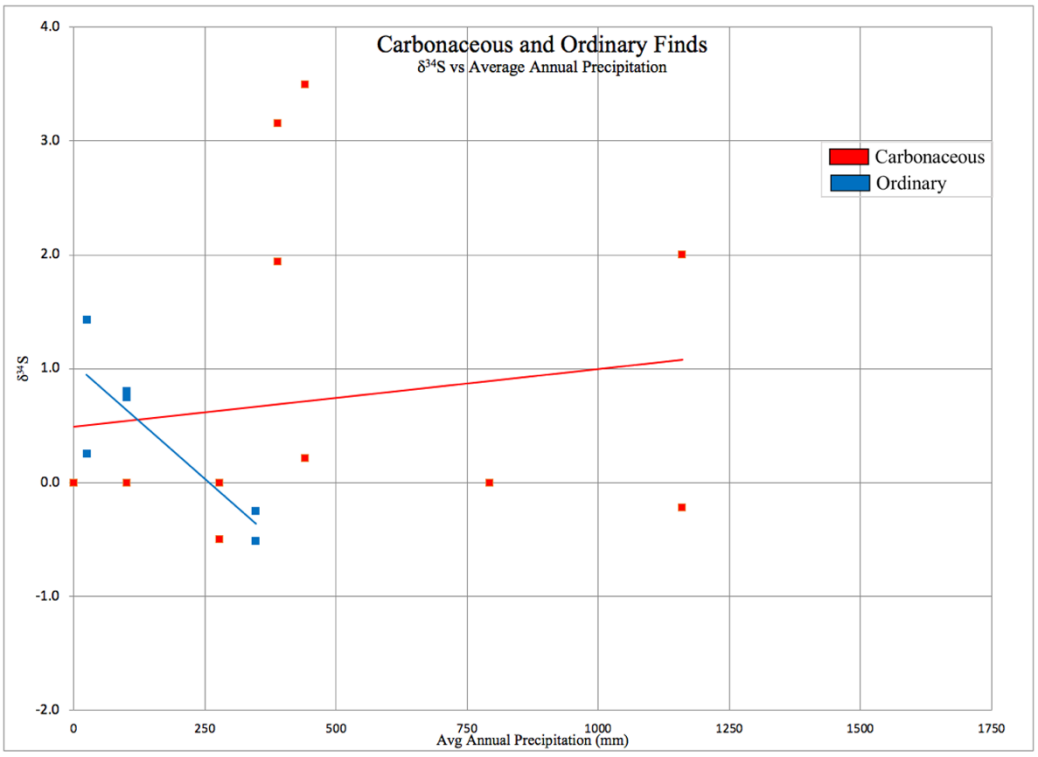

Figure 33. $\delta^{34}S$ versus average annual precipitation values (in millimeters) in all analyzed chondrite finds.

Sulfur data were also compared to average annual temperature at the impact site of each chondrite. A global impact site map overlain with a basemap displaying mean temperature for the month of July for years 1950-2000 (Figure 34) also demonstrates the wide range of temperature conditions the chondrites were exposed to in the field.

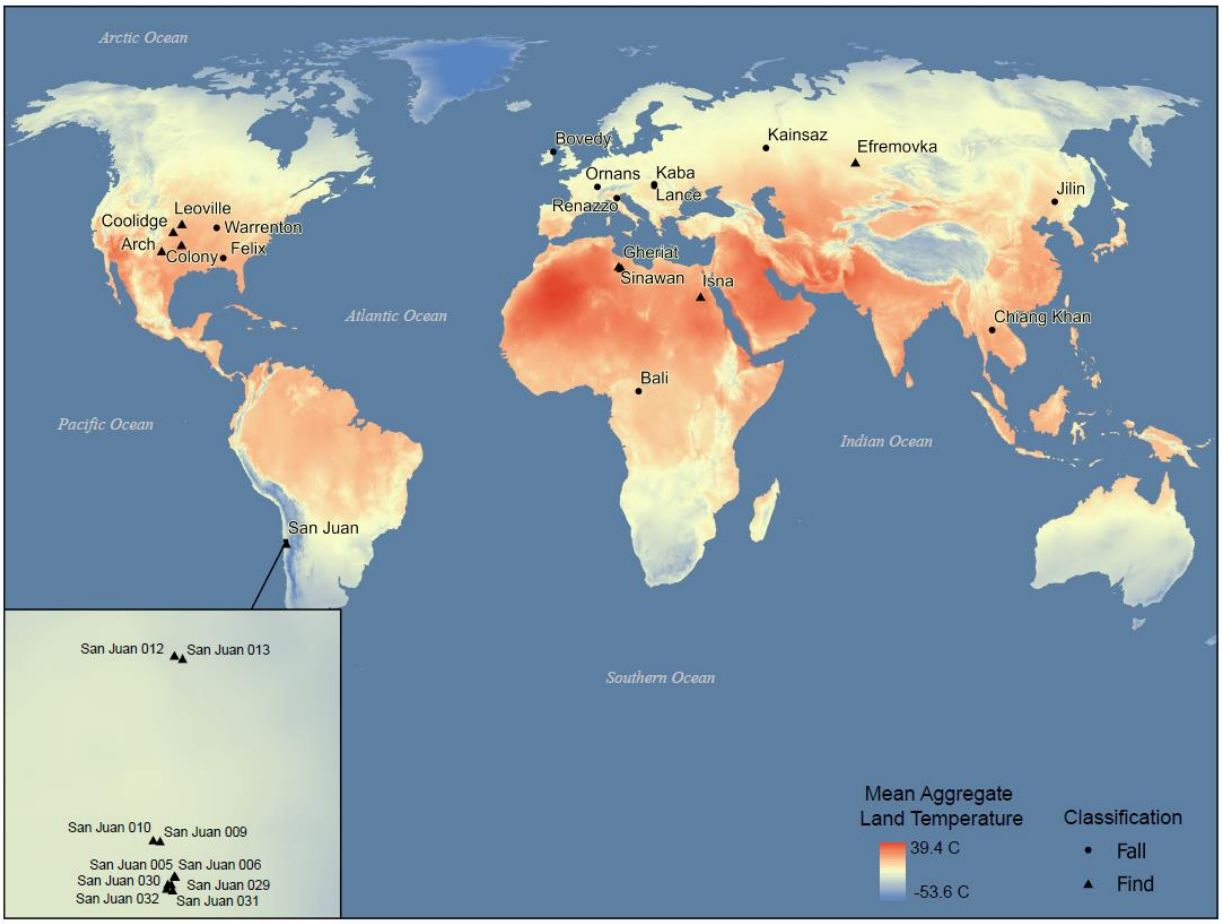

Figure 34. Global map of impact locations of the meteorites used in the S study. The basemap shows mean temperature in July from 1950-2000 using data from WorldClim Global Climate Data.

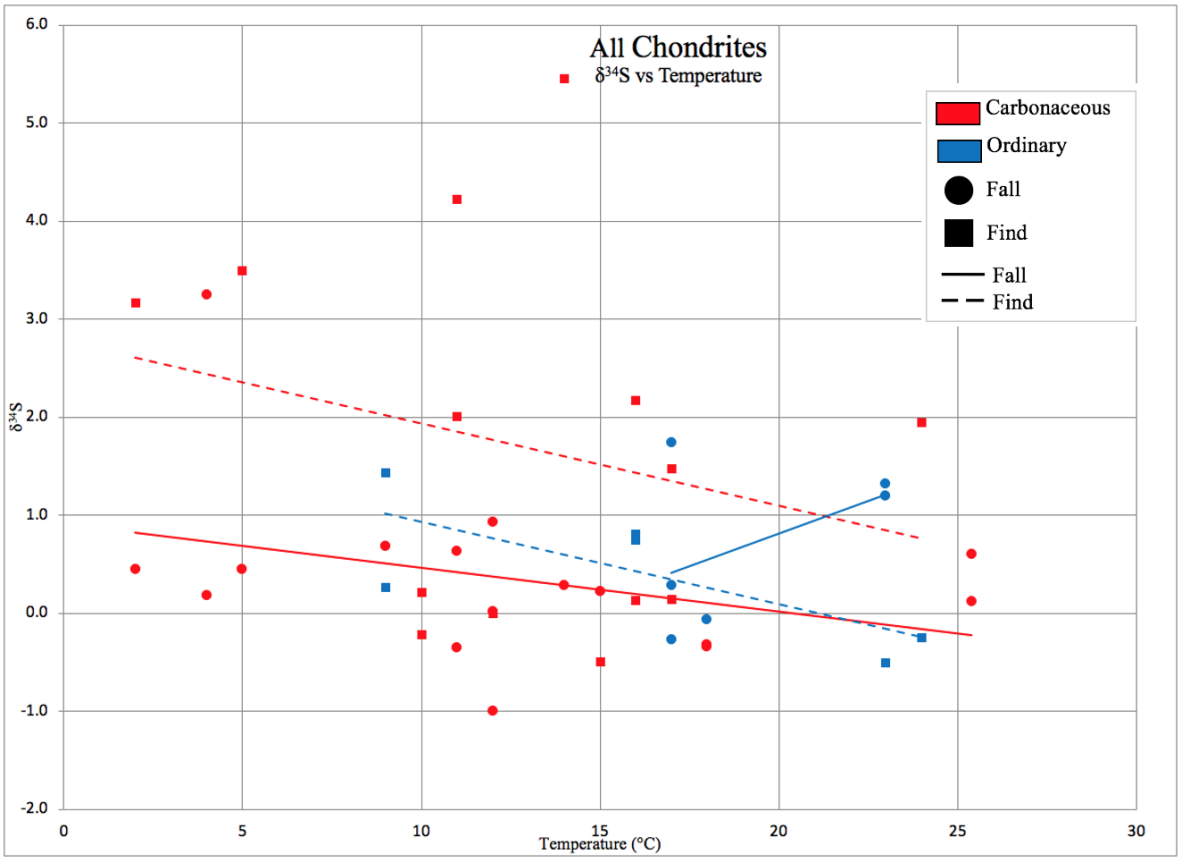

Figure 35. $\delta^{34}S$ versus average annual temperature values in all analyzed chondrite falls (circle) and finds (square) show little variance between carbonaceous (red) and ordinary (blue) groups. Most ordinary type samples were harvested from the same field site and experienced identical temperature conditions throughout the year.

The data were compared to average annual temperatures experienced at each respective impact site to assess the potential effect of heat fluctuations on chondritic S signatures (Figures 36, 37). In this case, carbonaceous falls and finds display trendlines with similar slopes, regardless of the presumed time spent in the field. The difference, however, lies within the intercept values. Carbonaceous falls display a small range of S isotope values around 0.0‰ (Figure 36), while carbonaceous finds display a greater variance of values averaging roughly 3.0‰ (Figure 37). This could be interpreted as temperature, in conjunction with locally-present precipitation, created a more powerful S-mobilizing reagent that fractionated S-bearing

compounds when allowed to reside in the field for an extended length of time (or at least longer than the time a fall spends in the field). The data from the ordinary type group contained multiple finds from the same meteorite field. To avoid skewing the dataset by displaying multiple ordinary falls with identical impact site temperatures, their values were averaged and displayed as singular points on the graph. An explanation of the wayward trendline of ordinary finds shown in Figure 36 is the study did not contain ordinary chondrites harvested from impact sites experiencing <16 ºC average annual temperature.

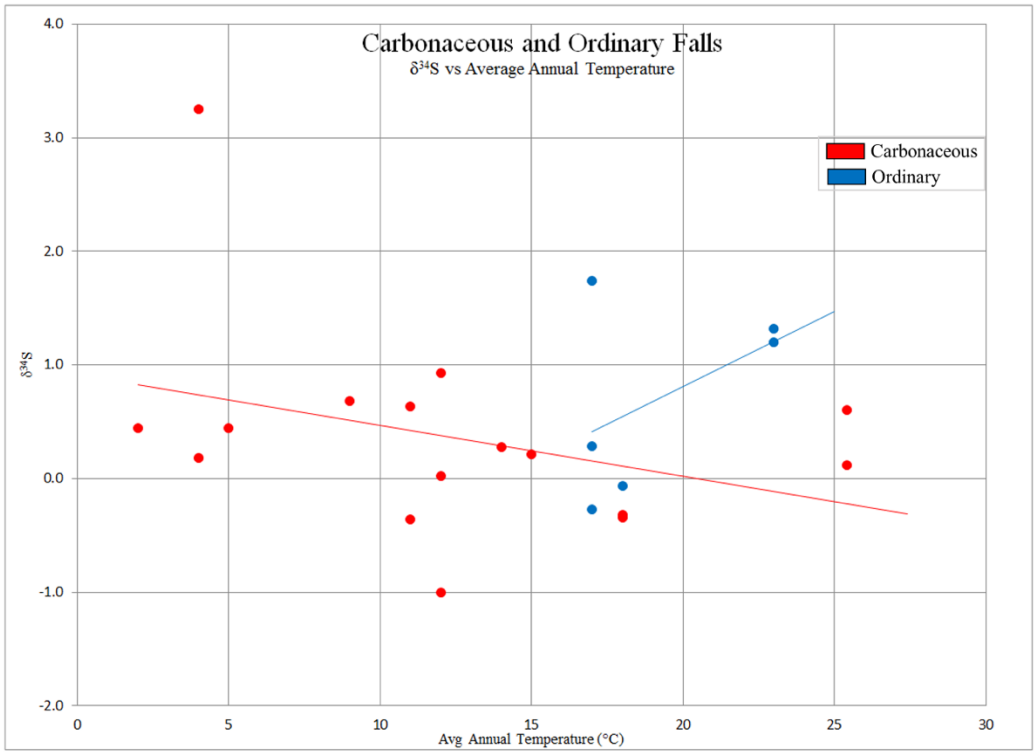

Figure 36. $\delta^{34}S$ versus average annual temperature values in all analyzed chondrite falls show variance between carbonaceous (red) and ordinary (blue) groups.

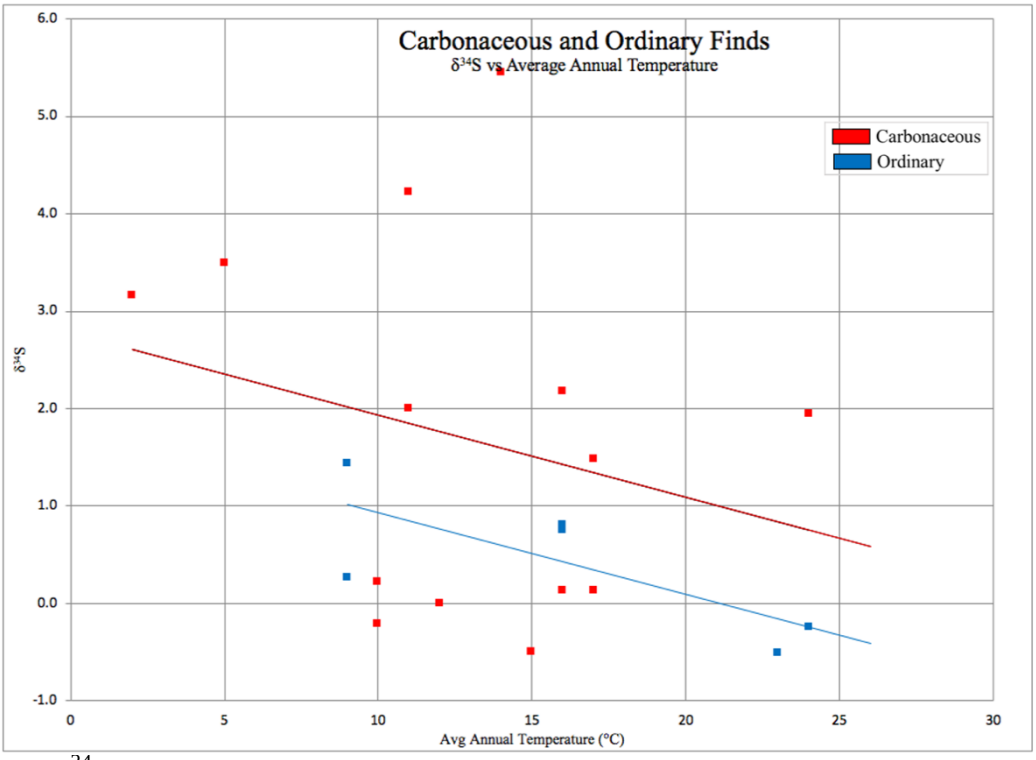

Figure 37. $\delta^{34}S$ versus average annual temperature values in all analyzed chondrite finds show little variance between carbonaceous (red) and ordinary (blue) groups.

V. CONCLUSION AND FUTURE DIRECTIONS

Meteorites are the gateway to understanding the origins of the solar system and formation of our home planet. It is essential to understand the degredation and weathering processes they undergo when subjected to terrestrial conditions in order to understand their original extraterrestrial compositions. The first part of this study examines concentrations of REE within magnetic and non-magnetic fractions of carbonaceous and ordinary chondrites. The data from the REE study show various elemental concentration anomalies (ie Eu, Nd, and Tm) for select data series. These anomalous values, though not contained within any one sub-division of chondrite categories, may provide insight into general extraterrestrial formation conditions as well as indicate mineral phases within the chondritic material.

The second part of this study examined the links between $\delta^{34}S$, S content, and terrestrial residence time. A key finding of this study shows falls and finds chondrites exhibit varying $\delta^{34}S$ isotopic signatures depending on the length of time a chondrite has resided in the field. Additional atmospheric variables such as temperature and precipitation are closely related to the mobility of S species within chondritic material, as was demonstrated by this study.

Future Directions

In addition to the rare earth elements, tellurium (Te) and selenium (Se) were examined for their concentrations within the chondrites. The concentrations of these two elements may be markers for supernova triggering processes during the formation of the solar system, so the employment of the unused data may be a worthwhile scientific endeavor to pursue.

The sulfur study should be expanded to include ordinary chondrites harvested from impact sites that are cold (<16 ºC) year round and also those which experience great amounts of

annual precipitation. Inclusion of samples fitting that description will enhance the validity of the findings and create a 'well-rounded' dataset.

The sulfur study should be expanded upon by using only bulk composition samples of chondrites with experimentally-derived terrestrial residence times. There is great potential for more detailed correlation of isotopic signatures and sulfur content with temperature and environmental moisture content by obtaining highly accurate and ongoing climate data from impact sites. This approach may be able to isolate the more influential of the two environmental characteristics on the $\delta^{34}S$ and $e^{(\%S)}$ results in the studied meteorite population, creating a more precise original meteorite chemical composition. Additionally, the S data needs to be compared to radioisotope data for the same meteorites used in the study to further verify the findings of the study.

Destruction of a meteorite is dependent on many factors including presence of a fusion crust, porosity, metal content, environmental moisture, temperature, carbon dioxide, soil chemistry, and vegetation (Buddhue, 1957). This study did not examine all of the aforementioned factors which play into meteorite degradation, leaving much room for continued work to be performed in this field of study.

REFERENCES

Aldrich, Sigma. “Sulfanilamide 46874.” *Sulfanilamide Analytical Standard*, Sigma-Aldrich, 2019, www.sigmaaldrich.com/catalog/product/sial/46874?lang=en&region=US.

Ayangbenro, Ayansina S et al. “Sulfate-Reducing Bacteria as an Effective Tool for Sustainable Acid Mine Bioremediation.” *Frontiers in microbiology* vol. 9 1986. 22 Aug. 2018, doi:10.3389/fmicb.2018.01986

Bea, Fernando. “Geochemistry of the Lanthanide Elements.” *SE Mineral*, 2004, www.semineral.es/websem/PdfServlet?mod=archivos&subMod=publicaciones&archivo=SeminSEMv12p5-12.pdf.

Bland, P. A., et al. "Weathering of chondritic meteorites." *Meteorites and the early solar system II* 1 (2006): 853-867.

Bland, P.A., et al. “Climate and Rock Weathering: a Study of Terrestrial Age Dated Ordinary Chondritic Meteorites from Hot Desert Regions.” *Geochimica Et Cosmochimica Acta*, vol. 62, no. 18, 1998, pp. 3169–3184., doi:10.1016/s0016-7037(98)00199-9.

Buddhue, John Davis. *The Oxidation and Weathering of Meteorites*. University of New Mexico Press, 1957.

Cronin, J. R., S. Pizzarello, and D. P. Cruikshank. 1988. Organic matter in carbonaceous chondrites, planetary satellites, asteroids and comets. In *Meteorites and the early solar system*, ed. J. F. Kerridge and M. S. Matthews, pp. 819–857. Tucson, Arizona: University of Arizona Press.

Dreibus, G., et al. “Sulfur and Selenium in Chondritic Meteorites.” *Meteoritics*, vol. 30, no. 4, 1995, pp. 439–445., doi:10.1111/j.1945-5100.1995.tb01150.x.

Evensen, N.M., et al. “Rare-Earth Abundances in Chondritic Meteorites.” *Geochimica Et Cosmochimica Acta*, Pergamon, 25 Mar. 2003, www.sciencedirect.com/science/article/pii/001670377890114X.

“Isotope Geology of Neodymium and Strontium in Igneous Rock.” *Principles of Isotope Geology*, by Gunter Faure, 2nd ed., John Wiley & Sons, 1986, pp. 217–238.

Gao, Xia, and Mark H. Thiemens. “Isotopic Composition and Concentration of Sulfur in Carbonaceous Chondrites.” *Geochimica Et Cosmochimica Acta*, vol. 57, no. 13, 1993, pp. 3159–3169., doi:10.1016/0016-7037(93)90300-l.

Gao, Xia, and Mark H. Thiemens. “Variations of the Isotopic Composition of Sulfur in Enstatite and Ordinary Chondrites.” *Geochimica Et Cosmochimica Acta*, vol. 57, no. 13, 1993, pp. 3171–3176., doi:10.1016/0016-7037(93)90301-c.

Gattacceca, Jérôme, et al. “The Densest Meteorite Collection Area in Hot Deserts: The San Juan Meteorite Field (Atacama Desert, Chile).” *Meteoritics & Planetary Science*, vol. 46, no. 9, 2011, pp. 1276–1287., doi:10.1111/j.1945-5100.2011.01229.x.

Greenwood, R. C., and I. A. Franchi. “Alteration and Metamorphism of CO3 Chondrites: Evidence from Oxygen and Carbon Isotopes.” *Meteoritics & Planetary Science*, vol. 39, no. 11, 2004, pp. 1823–1838., doi:10.1111/j.1945-5100.2004.tb00078.x.

Grossman, J. N. & Wasson, J. T. (1983), The compositions of chondrules in unequilibrated chondrites an evaluation of models for the formation of chondrules and their precursor materials, in E. A. King, ed., ‘Chondrules and their Origins’, pp. 88–121.

Hoefs, Jochen. *Stable Isotope Geochemistry*. 7th ed., Springer, 2019.

Hulston, J. R., and H. G. Thode. “Variations in the S33, S34, and S36contents of Meteorites and Their Relation to Chemical and Nuclear Effects.” *Journal of Geophysical Research*, vol. 70, no. 14, 1965, pp. 3475–3484., doi:10.1029/jz070i014p03475.

Hut, G., Consultants' group meeting on stable isotope reference samples for geochemical and hydrological investigations, 16-18 Sep. 1985. Report to the Director General, International Atomic Energy Agency, Vienna (1987).

Inglis-Arkell, Esther. “The Oddo-Harkins Rule Shows the Universe Hates the Odd.” *Gizmodo*, io9, 16 Dec. 2015, io9.gizmodo.com/the-oddo-harkins-rule-shows-the-universe-hates-the-odd-1446581327.

Jones, R. H. (2012), ‘Petrographic constraints on the diversity of chondrule reservoirs in the protoplanetary disk’, Meteoritics and Planetary Science 47, 1176–1190.

Jull, A. J. Timothy, et al. “Terrestrial Ages of Meteorites from the Nullarbor Region, Australia, Based on 14C and 14C-10Be Measurements.” *Meteoritics & Planetary Science*, vol. 45, no. 8, 2010, pp. 1271–1283., doi:10.1111/j.1945-5100.2010.01289.x.

Kaplan, I.r, and J.r Hulston. “The Isotopic Abundance and Content of Sulfur in Meteorites.” *Geochimica Et Cosmochimica Acta*, vol. 30, no. 5, 1966, pp. 479–496., doi:10.1016/0016-7037(66)90059-7.

“Chapter 2: Fundamentals of Isotope Geochemistry.” *Isotope Tracers in Catchment Hydrology*, by Carol Kendall and Jeffry J. McDonnell, Elsevier, 2006, pp. 53–84.

Labidi, J., et al. “Mass Independent Sulfur Isotope Signatures in CMs: Implications for Sulfur Chemistry in the Early Solar System.” *Geochimica Et Cosmochimica Acta*, vol. 196, 2017, pp. 326–350., doi:10.1016/j.gca.2016.09.036.

Labidi, Jabrane & König, S & Kurzawa, Timon & Yierpan, Aierken & Schoenberg, Ronny. (2018). The selenium isotopic variations in chondrites are mass-dependent; Implications for sulfide formation in the early solar system. Earth and Planetary Science Letters. 481. 212-222. 10.1016/j.epsl.2017.10.032.

Macke, Robert J., et al. "Density, Porosity, and Magnetic Susceptibility of Carbonaceous Chondrites." *Meteoritics & Planetary Science*, vol. 46, no. 12, 2011, pp. 1842–1862., doi:10.1111/j.1945-5100.2011.01298.x.

McDonald, John. "Handbook of Biological Statistics." *Wilcoxon Signed-Rank Test - Handbook of Biological Statistics*, 2013, www.biostathandbook.com/wilcoxonsignedrank.html.

McSween, Harry Y. *Meteorites*, 2003, web.gps.caltech.edu/classes/ge133/reading/meteorites_mcsween.pdf.

Meteoritical Bulletin, RSS. "Meteoritical Bulletin." *Meteoritical Bulletin RSS*, Lunar Planetary Institue, 2019, www.lpi.usra.edu/meteor/metbull.php?code=18030.

Norton, O. R. 2002. *The Cambridge encyclopedia of meteorites*. Cambridge, United Kingdom: Cambridge University Press.

Papike, James J. *Planetary Materials*. Vol. 36, Mineralogical Soc. of America, 1998.

Patzer, Andrea, et al. "Chondritic Ingredients: I. Usual Suspects and Some Oddballs in the Leoville CV3 Meteorite." *Meteoritics & Planetary Science*, vol. 47, no. 1, 2012, pp. 142–157., doi:10.1111/j.1945-5100.2011.01318.x.

Perkins, Sid. "Attack of the Rock-Eating Microbes." *Pearson - Science News*, 2003, www.phschool.com/science/science_news/articles/attack_rock_eating.html.

Rai, Vinai K., and Mark H. Thiemens. "Mass Independently Fractionated Sulfur Components in Chondrites." *Geochimica Et Cosmochimica Acta*, vol. 71, no. 5, 2007, pp. 1341–1354., doi:10.1016/j.gca.2006.11.033.

Robinson, B.W., "Sulphur isotope standards", Reference and intercomparison materials for stable isotopes of light elements, Proceedings of a consultants' meeting held in Vienna, 1-3. Dec. 1993, IAEA-TECDOC-825, IAEA, Vienna, Austria (1995) 39-45.

Saunier, Gaille. "Carbonaceous Chondrites." *Meteorite.fr - Classification - Stony Meteorites - Carbonaceous Chondrites*, 1998, www.meteorite.fr/en/classification/carbonaceous.htm.

Scherer, P., et al. "Allan Hills 88019: An Antarctic H- chondrite with a very long terrestrial age." *Meteoritics & Planetary Science* 32.6 (1997): 769-773.

Scott, E.R.D., and A.N. Krot. "Chondrites and Their Components." *Treatise on Geochemistry*, 2014, pp. 65–137., doi:10.1016/b978-0-08-095975-7.00104-2.

Sharp, Zachary. “Chapter 13: Extraterrestrial Materials.” *Principles of Stable Isotope Geochemistry*, Pearson Prentice Hall, 2007, pp. 351–380.

State, Penn. “S.3.2 Hypothesis Testing (P-Value Approach): STAT ONLINE.” *PennState: Statistics Online Courses*, 2019, onlinecourses.science.psu.edu/statprogram/reviews/statistical-concepts/hypothesis-testing/p-value-approach.

Welten, K. C., et al. "Lewis Cliff 86360: An Antarctic L- chondrite with a terrestrial age of 2.35 million years." *Meteoritics & Planetary Science* 32.6 (1997): 775-780.

Welten, K. C., et al. “Exposure History and Terrestrial Ages of Ordinary Chondrites from the Dar Al Gani Region, Libya.” *Meteoritics & Planetary Science*, vol. 39, no. 3, 2004, pp. 481–498., doi:10.1111/j.1945-5100.2004.tb00106.x.

White, William. “Chapter 10: The Big Picture: Cosmochemistry.” *Geochemistry*, John Wiley & Sons, 2013, pp. 421–483.